

Enhanced stripe phases in spin-orbit-coupled Bose-Einstein condensates in ring cavities

Farokh Mivehvar and David L. Feder*

*Institute for Quantum Science and Technology, Department of Physics and Astronomy,
University of Calgary, Calgary, Alberta, Canada T2N 1N4*

(Dated: June 18, 2021)

The coupled dynamics of the atom and photon fields in optical ring cavities with two counter-propagating modes give rise to both spin-orbit interactions as well as long-ranged interactions between atoms of a many-body system. At zero temperature, the interplay between the two-body and cavity-mediated interactions determines the ground state of a Bose-Einstein condensate. In this work, we find that cavity quantum electrodynamics in the weak-coupling regime favors a stripe-phase state over a plane-wave phase as the strength of cavity-mediated interactions increases. Indeed, the stripe phase is energetically stabilized even for condensates with attractive intra- and inter-species interactions for sufficiently large cavity interactions. The elementary excitation spectra in both phases correspond to linear dispersion relation at long wavelengths, indicating that both phases exhibit superfluidity, though the plane-wave phase also displays a characteristic roton-type feature. The results suggest that even in the weak coupling regime cavities can yield interesting new physics in ultracold quantum gases.

I. INTRODUCTION

The experimental realization of Bose-Einstein condensation (BEC) has opened many opportunities for realizing new many-body phases [1–3]. Ultracold atoms trapped in laser-generated optical lattice potentials experience crystalline environments and exhibit a variety of intriguing phenomena [4], most notably the superfluid–Mott-insulator phase transition [5]. There are numerous proposals for inducing gauge fields in quantum gases by means of laser light [6], and recently abelian [7] and non-abelian [8] gauge fields have been realized. In the latter work an equal combination of Rashba and Dresselhaus spin-orbit (SO) couplings were induced via two-photon Raman transitions. These developments have set the stage for realizing topological states in these systems [9].

The single-particle energy dispersion of a SO-coupled atom is a momentum-space double well, which is two-fold degenerate in the symmetric case [7]. In a Bose-Einstein condensate (BEC) of atoms, the two-body interactions lift this degeneracy and drive the BEC into either a plane wave phase (PWP) or a stripe phase (SP), depending on the strength and sign of the intra- and inter-species two-body interactions [10–13]. In the PWP, all atoms condense into one of the two single-particle energy minima, while the SP is a superposition state of the minima and the total BEC density exhibits faint fringes [14]. Additional phases are found for fully three-dimensional SO interactions [15]. When a SO-coupled quantum gas is confined in an optical lattice, the ground state of the system exhibits a variety of magnetic orderings in the Mott-insulator regime, such as ferromagnetic, antiferromagnetic, spin spiral, vortex and antivortex crystals, and skyrmion crystal phases [16–18]. The superfluid to Mott-

insulator phase transition of SO-coupled quantum gases has also been investigated [16, 19].

In laser-based approaches to generating SO couplings, the radiation field is treated classically and one ignores the back-action of the atoms on it. Confining the radiation field to within an optical cavity leads to a coherent exchange of energy and momentum between atoms and photons [20]. The back-action of the atoms on the photon fields is no longer negligible, leading to complex coupled dynamics of the matter and radiation fields in which both entities are affected by one another and must be treated on the same footing [21]. As a consequence, cavity-mediated long-range interactions are induced between atoms, yielding novel collective phenomena in atomic systems [22]. A few schemes have been recently proposed to induce SO coupling in ultracold atoms via quantum electrodynamics [23–26] and to couple a laser-induced SO-coupled BEC to the cavity field [27]. These schemes exhibit a wealth of physics, including strong synthetic magnetic fields, a cavity-mediated Hofstadter spectrum, and a variety of magnetic orders.

In this work we investigate the ground state and the elementary excitations of a spinor BEC at zero temperature subject to ring-cavity-induced SO interactions [23]. Here we consider lossy cavities where a steady-state photon population is maintained by the application of external pump lasers. The cavity photons mediate infinite-range interactions between atoms, whose strengths can be tuned experimentally by adjusting the amplitudes of the pump lasers. The sign of these interactions can be made positive or negative depending on the cavity detuning, the frequency difference between the applied pump lasers and the cavity. These cavity-mediated interactions compete with the inherent two-body interactions between atoms to determine the ground state of the SO-coupled BEC. In particular, stripe phases are always favored when positive cavity-mediated interactions dominate the two-body-interactions, even in the case where

*Corresponding author: dfeder@ucalgary.ca

the intrinsic atomic interactions (both intra- and inter-species) are attractive. Asymmetry in the strength of cavity-mediated interactions for different spin components yields stripe-phase states with an arbitrary number of atoms in the left or right minimum of the single-particle dispersion relation, so that the magnetization varies continuously from zero in the stripe phase to unity in the plane-wave phase. This behavior allows us to identify a novel stripe-phase order parameter, and to identify its associated mean-field critical exponent.

Consideration of the quantum fluctuations around the mean-field ground states reveals that the particle-hole elementary excitation spectra in both PWP and SP have the usual linear sound-like dispersion relation at long wavelengths, an indication of superfluidity. In the PWP, the dispersion relation also exhibits a roton-type feature at the same wave vector that characterizes the fringe periodicity in the SP, which could be used experimentally as a distinguishing feature. The critical transition between the PWP and SP occurs when the energy of this minimum falls below zero. Unlike for the PWP, in the SP the speed of sound depends strongly on the cavity-mediated interactions. The speed of sound is found fall below zero at a critical value of the cavity interactions and inter-species interactions strength, but this appears to signal a phase transition to a phase-separated state. Overall, the ring-cavity environment provides an experimentally convenient framework for exploring exotic ground states of SO-coupled BECs.

The manuscript is organized as follows. In Section II, we start from the full atom-photon Hamiltonian density for a lossy but pumped cavity, to derive an effective atomic Hamiltonian with the photon fields eliminated. The ground state of this effective Hamiltonian is explored in Section III using both a variational method and by solving the generalized Gross-Pitaevskii equations. The remainder of this Section is devoted to an analysis of the elementary excitations. A discussion of the results and conclusions are found in Sec. IV. Appendices A and B provide details of the adiabatic elimination of the atomic excited state and cavity fields, respectively.

II. MODEL AND HAMILTONIAN

Consider spin-1 bosonic atoms inside a ring cavity with two driven counter-propagating running modes $\hat{A}_1 e^{ik_1 z}$ and $\hat{A}_2 e^{-ik_2 z}$, where \hat{A}_j is the annihilation operator for the photon in j th mode with wave vector $k_j = \omega_j/c$ and z is the direction along the cavity axis. Without loss of generality, one can assume that the wave vectors k_1 and k_2 of the two modes are approximately equal to each other, $k_R \equiv k_1 \approx k_2$ [28]. The mode $\hat{A}_1 e^{ik_R z}$ ($\hat{A}_2 e^{-ik_R z}$) propagates to the right (left) and solely induces the atomic transition $|a\rangle \rightarrow |e\rangle$ ($|b\rangle \rightarrow |e\rangle$), where $\{|a\rangle, |b\rangle\}$ are non-degenerate pseudospin states of interest and $|e\rangle$ is an excited state. The two cavity modes \hat{A}_j are assumed to be sufficiently populated to justify omitting

associated degenerate modes \hat{A}'_j . In principle, a state-independent external potential $V_{\text{ext}}(\mathbf{r})$ would need to be imposed to confine atoms inside the cavity. The single-particle Hamiltonian density in the dipole and rotating-wave approximations is

$$\mathcal{H}^{(1)} = \mathcal{H}_{\text{at}}^{(1)} + H_{\text{cav}} + \mathcal{H}_{\text{ac}}^{(1)}, \quad (1)$$

with

$$\begin{aligned} \mathcal{H}_{\text{at}}^{(1)} &= \left[-\frac{\hbar^2}{2m} \nabla^2 + V_{\text{ext}}(\mathbf{r}) \right] I_{3 \times 3} + \sum_{\tau \in \{a,b,e\}} \varepsilon_{\tau} \sigma_{\tau\tau}, \\ H_{\text{cav}} &= \hbar \sum_{j=1,2} \omega_j \hat{A}_j^\dagger \hat{A}_j + i\hbar \sum_{j=1,2} \left(\eta_j \hat{A}_j^\dagger e^{-i\omega_{pj}t} - \text{H.c.} \right), \\ \mathcal{H}_{\text{ac}}^{(1)} &= \hbar \left[\left(\mathcal{G}_{ae} e^{ik_R z} \hat{A}_1 \sigma_{ea} + \mathcal{G}_{be} e^{-ik_R z} \hat{A}_2 \sigma_{eb} \right) + \text{H.c.} \right], \end{aligned}$$

where ε_{τ} are the internal atomic-state energies, $\sigma_{\tau\tau'} = |\tau\rangle \langle \tau'|$, and $I_{3 \times 3}$ is the identity matrix in the internal atomic-state space. The atom-photon coupling for the transition $\tau \leftrightarrow \tau'$ is denoted $\mathcal{G}_{\tau\tau'}$, and H.c. stands for the Hermitian conjugate. The cavity mode \hat{A}_j^\dagger is driven by a pump laser with frequency ω_{pj} and amplitude η_j , indicated by the second sum in H_{cav} . In this work, in order to simplify the analytical calculations, $V_{\text{ext}}(\mathbf{r})$ is set to zero. In reality, one might imagine a very weak (almost unbound) confining potential along the cavity axis z but a standard harmonic trap in the radial direction. The details of the transverse confining potential are not important for the analysis presented in this work.

After expressing Hamiltonian (1) in the rotating frame of the pump lasers [29] and assuming that the atomic detunings $\Delta_1 = \omega_1 - \varepsilon_{ea}/\hbar$ and $\Delta_2 = \omega_2 - \varepsilon_{eb}/\hbar$ are large compared to $\varepsilon_{ba}/\hbar = (\varepsilon_b - \varepsilon_a)/\hbar$, one can adiabatically eliminate the atomic excited state to obtain an effective Hamiltonian $\mathcal{H}_{\text{SO}}^{\prime(1)}$ for the ground pseudospin states $\{|1\rangle, |2\rangle\} \equiv \{|b\rangle, |a\rangle\}$. The details are presented in Appendix A. In the limit of a very weak confining potential along the cavity axis \hat{z} , one can assume that the momentum $p_z = \hbar k_z$ is a good quantum number. Alternatively one could consider approximately uniform quantum gases in a box potential where $V_{\text{ext}}(\mathbf{r}) = 0$ except at the boundaries; such a potential has recently been realized experimentally [30]. One can then transform to the co-moving frame of the cavity modes by applying the unitary transformation $\mathcal{U}_2 = e^{-ik_R z \sigma_z}$ (where $\sigma_z = \sigma_{11} - \sigma_{22}$ is the third Pauli matrix, see also Appendix A). The kinetic-energy part of the Hamiltonian density $\mathcal{H}_{\text{SO}}^{\prime(1)} \equiv \mathcal{U}_2 \mathcal{H}_{\text{SO}}^{\prime(1)} \mathcal{U}_2^\dagger$ associated with the momentum p_z , Eq. (A5), then takes the familiar form of an equal Rashba-Dresselhaus SO coupling: $\frac{1}{2m} (p_z I_{2 \times 2} + \hbar k_R \sigma_z)^2$, which is characterized by a double-well energy dispersion [8].

In the presence of dissipation, such as when the decay rate κ of both cavity modes is non-zero, one should in principle numerically solve the associated master equation [31]. That said, in the weak-coupling regime when

κ is the dominant energy scale, $\kappa \gg (\mathcal{G}_{ae}, \mathcal{G}_{be})$, the master equation approach is equivalent to including dissipation in the Heisenberg equations of motion for the cavity fields: $\partial_t \hat{A}_j = -i[\hat{A}_j, \mathcal{H}_{\text{SO}}^{(1)}]/\hbar - \kappa \hat{A}_j$ [21]. The cavity fields quickly reach steady states, allowing them to be adiabatically eliminated. Setting $\partial_t \hat{A}_j = 0$ one obtains steady-state expressions for \hat{A}_j that can be substituted into $\mathcal{H}_{\text{SO}}^{(1)}$ to yield an effective atomic Hamiltonian; the details are relegated to Appendix B.

The resulting effective many-body Hamiltonian reads

$$H_{\text{eff}} = \int d^3r \left(\hat{\Psi}^\dagger \mathcal{H}_{\text{SO}}^{(1)} \hat{\Psi} + \frac{1}{2} g_1 \hat{n}_1^2 + \frac{1}{2} g_2 \hat{n}_2^2 + g_{12} \hat{n}_1 \hat{n}_2 \right) + \sum_{\tau=1,2} U_\tau \hat{N}_\tau^2 + U_\pm \hat{S}_+ \hat{S}_- + U_\mp \hat{S}_- \hat{S}_+ + 2U_{\text{ds}} \hat{N} \hat{S}_x, \quad (2)$$

where $\hat{\Psi}(\mathbf{r}) = (\hat{\psi}_1(\mathbf{r}), \hat{\psi}_2(\mathbf{r}))^\top$ are the bosonic field operators obeying the commutation relation $[\hat{\psi}_\tau(\mathbf{r}), \hat{\psi}_{\tau'}^\dagger(\mathbf{r}')] = \delta_{\tau,\tau'} \delta(\mathbf{r} - \mathbf{r}')$, $\hat{N}_\tau = \int \hat{n}_\tau(\mathbf{r}) d^3r = \int \hat{\psi}_\tau^\dagger(\mathbf{r}) \hat{\psi}_\tau(\mathbf{r}) d^3r$ is the total atomic number operator for pseudospin $\tau \in \{1, 2\}$, $\hat{N} = \hat{N}_1 + \hat{N}_2$ is the total atomic number operator, and the x -component of the total spin operator is defined in a usual way $\hat{S}_x = \frac{1}{2}(\hat{S}_+ + \hat{S}_-)$ using the collective pseudospin raising and lowering operators $\hat{S}_+ = \hat{S}_-^\dagger = \int \hat{\psi}_1^\dagger(\mathbf{r}) \hat{\psi}_2(\mathbf{r}) d^3r$. The atoms in this system experience two kinds of interactions, reflected in the effective Hamiltonian H_{eff} : the standard two-body contact interactions and the cavity-mediated long-ranged interactions. Here $g_\tau \equiv g_{\tau\tau}$ denotes the two-body intra-species interaction strength and g_{12} the two-body inter-species interaction strength. The strength of the cavity-mediated interactions are found in Appendix B:

$$U_{1(2)} = \frac{4\hbar \mathcal{G}_0^4 \Delta_c (\Delta_c^2 - 3\kappa^2)}{\Delta^2 (\Delta_c^2 + \kappa^2)^3} \eta_{2(1)}^2, \\ U_{\pm(\mp)} = \frac{4\hbar \mathcal{G}_0^4 \Delta_c}{\Delta^2 (\Delta_c^2 + \kappa^2)^3} \left[\Delta_c^2 - \left(1 + 2 \frac{\eta_{2(1)}^2}{\eta_{1(2)}^2} \right) \kappa^2 \right] \eta_{1(2)}^2, \\ U_{\text{ds}} = \frac{4\hbar \mathcal{G}_0^4 \Delta_c (\Delta_c^2 - 3\kappa^2)}{\Delta^2 (\Delta_c^2 + \kappa^2)^3} \eta_1 \eta_2, \quad (3)$$

where $\mathcal{G}_0 \equiv \mathcal{G}_{ae} = \mathcal{G}_{be}$, $\Delta \equiv \Delta_1 = \Delta_2$, and $\Delta_c \equiv \omega_{pj} - \omega_j$. The single-particle part of the effective Hamiltonian density has the familiar form of the equal Rashba-Dresselhaus SO coupling:

$$\mathcal{H}_{\text{SO}}^{(1)} = -\frac{\hbar^2}{2m} \left[\nabla_\perp^2 - (-i\partial_z + k_R \sigma_z) \right]^2 + V_{\text{ext}}(\mathbf{r}) + \frac{1}{2} \hbar \delta \sigma_z + \hbar \Omega_R \sigma_x, \quad (4)$$

with the effective two-photon detuning and Raman cou-

pling given by (see Appendix B)

$$\delta = \frac{2\mathcal{G}_0^2 (\Delta_c^2 - \kappa^2)}{\Delta (\Delta_c^2 + \kappa^2)^2} (\eta_2^2 - \eta_1^2), \\ \Omega_R = \frac{2\mathcal{G}_0^2 (\Delta_c^2 - \kappa^2)}{\Delta (\Delta_c^2 + \kappa^2)^2} \left[1 - \frac{2\mathcal{G}_0^2 \Delta_c}{\Delta (\Delta_c^2 - \kappa^2)} \right] \eta_1 \eta_2. \quad (5)$$

Before proceeding further, consider briefly some realistic order-of-magnitude estimates for various parameters used in the theory based on current experiments in ultracold atomic gases and cavity QED. The first experimental realization of a synthetic SO coupling was carried out on ^{87}Rb atoms using two counter-propagating Raman laser beams with wavelength $\lambda_R = 804.1$ nm ($E_R = 2.33 \times 10^{-30}$ J) [8]; the two-body interaction strengths for the desired pseudospin states of ^{87}Rb atoms are reported to be $g_1 = 5.009 \times 10^{-51}$ Jm³ and $g_2 = g_{12} = 4.986 \times 10^{-51}$ Jm³. With typical average BEC densities \bar{n} of order $10^{20} - 10^{21}$ m⁻³ [2], one obtains $g_\tau \bar{n} / E_R \sim 1$.

One might reasonably expect interesting physics to emerge when the strength of cavity-mediated interactions becomes comparable to the intrinsic inter-particle interactions, i.e. when $VU_\tau / g_\tau \sim 1$. Most experimental work is focused on the strong-cavity limit, where $\mathcal{G} \gg \kappa$; typical atom-cavity coupling and cavity decay rates for ^{87}Rb are $\mathcal{G}_{ae} \sim \mathcal{G}_{be} \sim 10\kappa \sim 2\pi \times 10$ MHz [32, 33]. One can attain $VU_\tau / g_\tau \sim 1$ by choosing $\Delta \sim 26$ THz, $\eta_1 = \eta_2 = -\Delta_c = 10$ MHz (for example, $\Delta_c \approx 28\kappa$ and $\eta \approx 2.2\kappa$ in Ref. 32), and a volume $V = 10^{-4}$ mm³; for these parameters one also obtains $\hbar\Omega_R / E_R \sim 4 \times 10^{-3}$. The weak coupling regime relevant to the present work can be attained by increasing the value of κ , for example by decreasing the reflectivity of the cavity mirrors. Choosing $\kappa \sim 2\pi \times 100$ MHz one can nevertheless ensure $VU_\tau / g_1 \sim 1$ choosing a larger volume $V = 10^{-3}$ mm³ as well as stronger pump fields and cavity detuning $\eta_1 = \eta_2 = -3\Delta_c = 3$ GHz; these choices yield $\hbar\Omega_R / E_R \sim 4 \times 10^{-2}$. Further increasing the driving field intensities up to $\eta_1 = \eta_2 = 15$ GHz at the fixed $\Delta_c = -1$ GHz results in cavity-mediated interactions that are an order of magnitude larger than the two-body interactions $VU_\tau / g_1 \sim 30$ while $\hbar\Omega_R / E_R \sim 1$.

In Appendix B, which discusses the adiabatic elimination of the cavity fields and the origin of the long-ranged cavity interactions, quantities such as $\mathcal{G}_0^2 / [\Delta(\Delta_c + i\kappa)]$ and $\mathcal{G}_0^2 N_\tau / [\Delta(\Delta_c + i\kappa)]$ are assumed to be small. Using the weak-coupling values considered above and assuming a typical average BEC particle number $N_\tau \sim 10^5$, it is straightforward to verify that both $\mathcal{G}_0^2 / |\Delta(\Delta_c + i\kappa)| \ll 1$ and $\mathcal{G}_0^2 N_\tau / |\Delta(\Delta_c + i\kappa)| \sim 10^{-2} \ll 1$. Making use of $\kappa \ll \Delta_c$ and defining $\xi \equiv 2\mathcal{G}_0^2 / \Delta \Delta_c \ll 1$, one can write

$$\Omega_R \approx \frac{\xi \eta_1 \eta_2}{\Delta_c}; \quad \delta \approx \frac{\xi}{\Delta_c} (\eta_2^2 - \eta_1^2); \quad U_{\text{ds}} \approx \frac{\hbar \xi^2}{\Delta_c} \eta_1 \eta_2; \\ U_{1(2)} = U_{\mp(\pm)} \approx \frac{\hbar \xi^2}{\Delta_c} \eta_{1(2)}^2. \quad (6)$$

If $\eta_1 = \eta_2$ then $\hbar\delta = 0$ and $U_{\text{ds}} = U_{1(2)} = U_{\mp(\pm)}$ with $U_1 / \hbar\Omega_R = \xi \ll 1$. Alternatively, if both pump fields are

non-zero ($\eta_1, \eta_2 \neq 0$), then defining $\delta U \equiv U_2 - U_1$ one obtains $\delta U/\hbar\delta = U_{\text{ds}}/\hbar\Omega_R = \xi \ll 1$. These relations will be important below when choosing parameters for the theoretical calculations.

III. GROUND STATE AND EXCITATIONS: ANALYTICS

The above analysis indicates that as long as η_1 and η_2 are not too different from one another then $\delta \ll \Omega_R$; in the following we therefore restrict calculations to $\delta \simeq 0$. The effective single-particle Hamiltonian can be diagonalized, and expressed in the form $H_{\text{SO}}^{(1)} = \sum_{\mathbf{k}, \lambda=\pm} \epsilon_{\lambda}(\mathbf{k}) \hat{\varphi}_{\lambda}^{\dagger}(\mathbf{k}) \hat{\varphi}_{\lambda}(\mathbf{k})$ with single-particle energy dispersion relation

$$\tilde{\epsilon}_{\pm}(\tilde{\mathbf{k}}) \equiv \frac{\epsilon_{\pm}(\mathbf{k})}{E_R} = \tilde{k}^2 + 1 \pm \sqrt{4\tilde{k}_z^2 + \tilde{\Omega}_R^2}, \quad (7a)$$

and spinor eigenstates

$$\phi_{-}(\mathbf{k}) = \begin{pmatrix} \sin \theta_{\mathbf{k}} \\ -\cos \theta_{\mathbf{k}} \end{pmatrix}; \quad \phi_{+}(\mathbf{k}) = \begin{pmatrix} \cos \theta_{\mathbf{k}} \\ \sin \theta_{\mathbf{k}} \end{pmatrix}, \quad (7b)$$

where ‘+’ and ‘-’ designate the upper and lower band, respectively, and $\sin 2\theta_{\mathbf{k}} = \tilde{\Omega}_R/\sqrt{4\tilde{k}_z^2 + \tilde{\Omega}_R^2}$. The unitless parameters $\tilde{\mathbf{k}} = \mathbf{k}/k_R$ and $\tilde{\Omega}_R = \hbar\Omega_R/E_R$ are defined for convenience, where $E_R = \hbar^2 k_R^2/2m$ is the recoil energy. Recall that using experimentally motivated parameters as discussed toward the end of Sec. II, one can choose $\tilde{\Omega}_R \sim \mathcal{O}(1)$. Note that in deriving this result we have assumed that the condensate is confined in a box potential with negligible occupation of transverse momentum states, i.e. $\mathbf{k} = (0, 0, \tilde{k}_z)$. In fact, the nature of the transverse confinement is not important in the current work; for example, instead assuming a strong radial oscillator potential $V(\rho) = m\omega_{\rho}^2 \rho^2/2$ one would simply replace \tilde{k}^2 by $\tilde{k}_z^2 + \hbar\omega_{\rho}/E_R$ under the assumption that the condensate occupied the ground state of the radial oscillator.

The energy dispersion with respect to \tilde{k}_z consists of two bands with a band gap of $2\tilde{\Omega}_R$ at the origin $\tilde{\mathbf{k}} = 0$. The lower energy band $\tilde{\epsilon}_{-}(\mathbf{k})$ is a symmetric double well along the \tilde{k}_z direction with the two minima located at

$$\tilde{k}_z = \pm \tilde{k}_0 \equiv \pm \sqrt{1 - \tilde{\Omega}_R^2/4}, \quad (8)$$

for $\tilde{\Omega}_R < 2$, and it has a single minimum at $\tilde{k}_z = 0$ when $\tilde{\Omega}_R > 2$ (the minima along the other two directions always occur at $\tilde{\mathbf{k}}_{\perp} = 0$). The operators $\hat{\Phi}(\mathbf{k}) = (\hat{\varphi}_{+}(\mathbf{k}), \hat{\varphi}_{-}(\mathbf{k}))^T$ annihilate a boson at momentum \mathbf{k} in the upper and lower bands and are related to the field operators through $\hat{\Psi}(\mathbf{r}) = \sum_{\mathbf{k}, \lambda=\pm} e^{i\mathbf{k}\cdot\mathbf{r}} \phi_{\lambda}(\mathbf{k}) \hat{\varphi}_{\lambda}(\mathbf{k})$. Note

that the laboratory-frame bosonic field operators $\tilde{\Psi}(\mathbf{r})$ (which gives the observable atomic density distribution) are related to $\hat{\Psi}(\mathbf{r})$ by the unity transformation \mathcal{U}_2 , i.e. $\tilde{\Psi}(\mathbf{r}) = \mathcal{U}_2^{\dagger} \hat{\Psi}(\mathbf{r})$.

The single-particle ground state of the symmetric double well (i.e. when $\tilde{\Omega}_R < 2$) is two-fold degenerate; the atom is either in the left minimum at $\tilde{\mathbf{k}} = -\tilde{\mathbf{k}}_0 = (0, 0, -\tilde{k}_0)$ or the right minimum at $\tilde{\mathbf{k}} = \tilde{\mathbf{k}}_0 = (0, 0, \tilde{k}_0)$. The non-interacting N -particle ground state, when the cavity-mediated interactions are also absent, is therefore $(N+1)$ -fold degenerate (any number of pseudospin-up atoms, up to N , can reside in the left well). Nonetheless, the two-body and cavity-mediated interactions compete with each other to lift this degeneracy.

A. Variational Approach

In order to determine the nature of the ground state, we assume the following ansatz for the BEC condensate wavefunction,

$$\begin{bmatrix} \psi_1 \\ \psi_2 \end{bmatrix} = \sqrt{\bar{n}} \left\{ c_1 e^{-ik_0 z} \begin{bmatrix} \cos \theta_{\mathbf{k}_0} \\ -\sin \theta_{\mathbf{k}_0} \end{bmatrix} + c_2 e^{ik_0 z} \begin{bmatrix} \sin \theta_{\mathbf{k}_0} \\ -\cos \theta_{\mathbf{k}_0} \end{bmatrix} \right\} \quad (9)$$

where $k_0 = k_R \tilde{k}_0$ and $\bar{n} = N/V$ is the average particle density, with N and V being the total particle number and volume, respectively. The variational parameters are c_1 and c_2 with the normalization constraint $|c_1|^2 + |c_2|^2 = 1$. Once they are determined, one can find the relevant ground-state quantities such as the total density $n(\mathbf{r}) = |\psi_1(\mathbf{r})|^2 + |\psi_2(\mathbf{r})|^2$, and the magnetization per particle $s_z(\mathbf{r}) = [|\psi_1(\mathbf{r})|^2 - |\psi_2(\mathbf{r})|^2]/\bar{n}$:

$$n(\mathbf{r}) = \bar{n} [1 + 2|c_1 c_2| \cos(2k_0 z + \gamma) \sin 2\theta_{\mathbf{k}_0}], \quad (10)$$

$$s_z(\mathbf{r}) = (|c_1|^2 - |c_2|^2) \cos 2\theta_{\mathbf{k}_0}, \quad (11)$$

where γ is the relative phase between c_1 and c_2 . Note that the magnetization s_z is homogeneous while the total density $n(\mathbf{r})$ exhibits fringes in the z direction provided that $c_1 c_2 \neq 0$. Constraining $\tilde{\Omega}_R < 2$, one can write $\sin 2\theta_{\mathbf{k}_0} = \tilde{\Omega}_R/2$ and $\cos 2\theta_{\mathbf{k}_0} = \tilde{k}_0$; then these take the simpler form $n(z) = \bar{n} [1 + \tilde{\Omega}_R |c_1 c_2| \cos(2k_0 z + \gamma)]$ and $s_z = \tilde{k}_0 (2|c_1|^2 - 1)$. The energy functional $E[c_1, c_2] = E_0 + E_{\text{int}}$ is obtained from Eq. (2) by replacing the field operators $\hat{\psi}_{\tau}$ with the corresponding condensate wavefunctions ψ_{τ} . This yields $E_0 = -N E_R \tilde{\Omega}_R^2/4$ and

$$E_{\text{int}} = \frac{N^2|g_1|}{4V} \left\{ \text{sgn}(g_1) + \tilde{g}_2 + 4\tilde{U}_1 + 2\delta\tilde{U} - 2\tilde{U}_{\text{ds}}\tilde{\Omega}_R + \left[2\tilde{g}_{12} - \text{sgn}(g_1) - \tilde{g}_2 + 4(\tilde{U}_{\text{ss}} - \tilde{U}_1) - 2\delta\tilde{U} \right] \frac{\tilde{\Omega}_R^2}{8} \right. \\ \left. + \frac{1}{2} (|c_1|^2 - |c_2|^2) \left(4 - \tilde{\Omega}_R^2 \right)^{1/2} [\text{sgn}(g_1) - \tilde{g}_2 - 2\delta\tilde{U}] \right. \\ \left. - 2|c_1c_2|^2 \left[\text{sgn}(g_1) + \tilde{g}_2 + 4\tilde{U}_1 + 2\delta\tilde{U} - 2\tilde{g}_{12} - \left(3\text{sgn}(g_1) + 3\tilde{g}_2 + 8\tilde{U}_1 + 4\delta\tilde{U} - 2\tilde{g}_{12} \right) \frac{\tilde{\Omega}_R^2}{8} \right] \right\}, \quad (12)$$

where the two-body interaction strengths are rescaled by $|g_1|$ (for example $\tilde{g}_2 = g_2/|g_1|$) and the cavity-mediated interaction strengths are rescaled by $|g_1|/V$ (for example $\tilde{U}_1 = VU_1/|g_1|$). In the above equations we have defined $2\tilde{U}_{\text{ss}} \equiv \tilde{U}_+ + \tilde{U}_\mp$ and $\delta\tilde{U} \equiv \tilde{U}_2 - \tilde{U}_1$, and $\text{sgn}(g_1) = g_1/|g_1| = \pm 1$ denotes the sign of g_1 . Again, recall that using experimentally motivated parameters as discussed toward the end of Sec. II, $\tilde{U}_{1(2)} \sim \tilde{\Omega}_R \sim \mathcal{O}(1)$. E_0 is the single-particle contribution to the energy and is independent of c_i , as expected. Minimizing E_{int} with respect to c_i determines the ground state of the system. The parameters \tilde{U}_1 and $\delta\tilde{U}$ (or \tilde{U}_2) are the only cavity-mediated interaction parameters having an effect on the ground state.

Consider first the simplest case where $\tilde{g}_2 = \text{sgn}(g_1)$ and $\delta\tilde{U} = 0$, so that only that last line of Eq. (12) contributes to the interaction energy. Then the energy is minimized either with $(c_1, c_2) = (1, 0)$ or $(0, 1)$, or with $c_1 = c_2 = 1/\sqrt{2}$ (neglecting relative phases). The first solution set corresponds to all atoms condensing in a single minimum of the single-particle energy dispersion (i.e. a single plane wave with wave vector $-\mathbf{k}_0$ or \mathbf{k}_0), labeled the plane wave phase (PWP). In the PWP the total density is uniform. The magnetization takes the value $s_z = \pm \tilde{k}_0 = \pm(1 - \tilde{\Omega}_R^2/4)^{1/2}$, with the upper (lower) sign corresponding to $c_1 = 1$ ($c_1 = 0$). For small $\tilde{\Omega}_R$ the magnetization approaches unity. Note that the PWP is twofold degenerate; that is, all atoms can condense in the left ($c_1 = 1$) or right minimum ($c_2 = 1$). The second solution set corresponds to atoms condensing into a superposition state of plane waves. It is characterized by the broken translational symmetry and the resulting density $n(z) = n[1 + \frac{1}{2}\tilde{\Omega}_R \cos(2k_0z + \gamma)]$ exhibits spatial variations in the z (i.e. SO-coupling) direction, so this is referred to as the stripe phase (SP). In this phase the density oscillations have greatest contrast for large $\tilde{\Omega}_R \rightarrow 2$. The SP magnetization s_z is zero.

The SP solution yields a lower energy than the PWP solution when term in square brackets in the last line of Eq. (12) is positive. (Recall $\tilde{g}_2 = \text{sgn}(g_1)$ and $\delta\tilde{U} = 0$ so that the middle line vanishes identically.) The cavity interaction strength that favors the SP solution is therefore

$\tilde{U}_1 > \tilde{U}_{1c}^0$, where

$$\tilde{U}_{1c}^0 \equiv \frac{8[\tilde{g}_{12} - \text{sgn}(g_1)] - [\tilde{g}_{12} - 3\text{sgn}(g_1)]\tilde{\Omega}_R^2}{4(4 - \tilde{\Omega}_R^2)}, \quad (13)$$

is the critical cavity interaction for the SP-PWP transition. In the limit of small $\tilde{\Omega}_R$, this becomes $\tilde{U}_{1c}^0 \simeq \frac{1}{2}[\tilde{g}_{12} - \text{sgn}(g_1)] + \frac{1}{16}[\tilde{g}_{12} + \text{sgn}(g_1)]\tilde{\Omega}_R^2$. If $\tilde{g}_{12} = \text{sgn}(g_1)$ the SP is favored for any non-zero, positive cavity interaction in the limit $\tilde{\Omega}_R \rightarrow 0$. In the other hand when $\tilde{\Omega}_R \rightarrow 2$ and $\tilde{g}_{12} \neq -\text{sgn}(g_1)$, the critical cavity interaction \tilde{U}_{1c}^0 diverges and SP is only favored for very large positive cavity interaction.

It is important to verify that the total interaction energy, Eq. (12), remains positive; the system is stable only if $\partial^2 E_{\text{int}}/\partial N^2 > 0$. Let us examine this first in the SP where $c_1 = c_2 = 1/\sqrt{2}$, for a special case where $\tilde{U}_{\text{ds}} = \tilde{U}_{\text{ss}} = \tilde{U}_1$ (and $\tilde{g}_2 = \text{sgn}(g_1)$ and $\delta\tilde{U} = 0$ as before). One obtains

$$E_{\text{int}} = \frac{N^2|g_1|}{4V} \left\{ \frac{1}{8} [\tilde{g}_{12} + \text{sgn}(g_1)] \left(8 + \tilde{\Omega}_R^2 \right) \right. \\ \left. + \frac{1}{2} \tilde{U}_1 \left(2 - \tilde{\Omega}_R \right)^2 \right\}. \quad (14)$$

Surprisingly, the SP is energetically stable for two-component attractive BECs in the presence of spin-orbit interactions as long as the inter-species interaction strength is sufficiently large and positive. Substituting the critical cavity interaction \tilde{U}_{1c}^0 into Eq. (14) yields the constraint

$$\tilde{g}_{12} \geq \text{sgn}(g_1) \frac{\tilde{\Omega}_R \left[(2 - \tilde{\Omega}_R)^2 - 12 \right]}{\tilde{\Omega}_R^3 + 16}. \quad (15)$$

In the limit of $\tilde{\Omega}_R \rightarrow 0$, for the lowest possible values of the cavity interaction favoring the SP phase $\tilde{U}_1 \gtrsim \tilde{U}_{1c}^0 = \frac{1}{2}[\tilde{g}_{12} - \text{sgn}(g_1)]$, the SP is energetically stable as long as $\tilde{g}_{12} \geq 0$, with no constraint on the sign of the intra-species interaction strength. Thus, the infinite-range cavity-mediated atom-atom interactions stabilize attractive two-component BECs against collapse, even in the absence of a confining potential. For larger values of \tilde{U}_1 even the inter-species interactions can be attractive.

The coefficient of \tilde{U}_1 in Eq. (14) is strictly positive. Therefore, for a given parameter set $\{\text{sgn}(g_1), \tilde{g}_{12}, \tilde{\Omega}_R\}$

one can choose arbitrary large positive values of the cavity interaction strength to strongly favor SP without compromising stability (i.e. to satisfy $\tilde{U}_1 > \tilde{U}_{1c}^0$ while ensuring that $E_{\text{int}} \geq 0$). In other words, the minimal cavity interaction \tilde{U}_1 which favors a stable SP satisfies

$$\tilde{U}_1 > \max \left\{ -\frac{[\tilde{g}_{12} + \text{sgn}(g_1)](8 + \tilde{\Omega}_R^2)}{4(2 - \tilde{\Omega}_R)^2}, \tilde{U}_{1c}^0 \right\}. \quad (16)$$

The stability of PWP can be investigated in a similar manner. The plane wave phase is favored when $\tilde{U}_1 < \tilde{U}_{1c}^0$. The positivity constraint of the interaction energy in the PWP

$$E_{\text{int}} = \frac{N^2|g_1|}{2V} \left\{ \text{sgn}(g_1) + \frac{1}{8} [\tilde{g}_{12} - \text{sgn}(g_1)] \tilde{\Omega}_R^2 + \tilde{U}_1 (2 - \tilde{\Omega}_R) \right\} > 0, \quad (17)$$

imposes a lower bound in the cavity interaction

$$-\frac{8 \text{sgn}(g_1) + [\tilde{g}_{12} - \text{sgn}(g_1)] \tilde{\Omega}_R^2}{8(2 - \tilde{\Omega}_R)} < \tilde{U}_1 < \tilde{U}_{1c}^0, \quad (18)$$

beyond which PWP is unstable. Thus, even the PWP becomes energetically stable for attractive spin-orbit coupled two-component BECs if the cavity-mediated interactions are judiciously chosen.

Figure 1 depicts the phase diagrams in the $\{\tilde{U}_1, \tilde{\Omega}_R\}$ and $\{\tilde{U}_1, \tilde{g}_{12}\}$ parameter planes. The phase diagrams are comprised of two physical regions: the SP and PWP, denoted by black and white in Fig. 1, respectively. The dark (light) grey indicates the regions where the SP (PWP) is energetically unstable. Figure 1(a) shows the phase diagram in the $\{\tilde{U}_1, \tilde{\Omega}_R\}$ parameter space for $\text{sgn}(g_1) = \tilde{g}_2 = 1$ and different values of \tilde{g}_{12} . The stripe phase is favored over an ever-larger parameter space as \tilde{U}_1 increases as long as $|\tilde{\Omega}_R| < 2$ to assure the existence of a double-well single-particle dispersion. This general trend is also evident from Fig. 1(b), the phase diagram in the $\{\tilde{U}_1, \tilde{g}_{12}\}$ parameter plane for $\text{sgn}(g_1) = \tilde{g}_2 = -1$ and constant $\tilde{\Omega}_R = 0.1$, where Eq. (13) reveals that the phase boundary is linear in \tilde{g}_{12} for fixed $\tilde{\Omega}_R$.

Relaxing the constraint considered above that $\delta\tilde{U} = 0$ in Eq. (12), one can prepare any arbitrary superposition state, i.e. arbitrary c_1 and c_2 subject to $|c_1|^2 + |c_2|^2 = 1$. The plane-wave phase is no longer degenerate; rather, the minimum favored depends on the sign of $\delta\tilde{U}$. Figure 2 shows the dependence of $|c_1|^2$ in the $\{\tilde{U}_{12}, \tilde{\Omega}_R\}$ plane for $\text{sgn}(g_1) = \tilde{g}_2 = \delta\tilde{U} = 1$, and $\tilde{g}_{12} = 2$. Under these conditions the SP with $|c_1| = |c_2|$ is found only for very large $\tilde{U}_1 \gg \tilde{U}_{1c}$, i.e. far from the SP-PWP phase boundary \tilde{U}_{1c} . Whereas for $\tilde{U}_1 \rightarrow \tilde{U}_{1c}^+$, $|c_1|^2$ increases monotonically until the PWP with $|c_1|^2 = 1$ is attained for $\tilde{U}_1 < \tilde{U}_{1c}$ (note that the critical value $\tilde{U}_{1c} \simeq \tilde{U}_{1c}^0$ and is weakly dependent on $\delta\tilde{U}$, as discussed below). The plane-wave

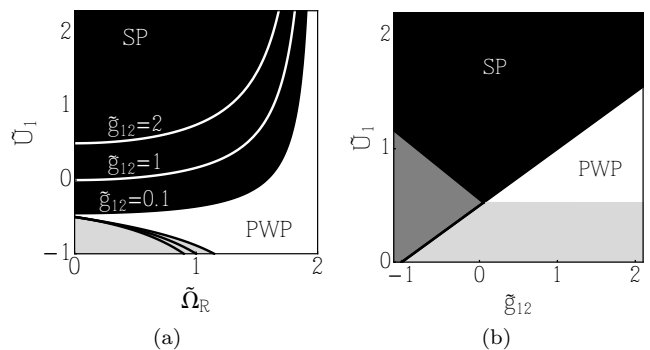


FIG. 1: Phase diagrams in the (a) $\{\tilde{U}_1, \tilde{\Omega}_R\}$ and (b) $\{\tilde{U}_1, \tilde{g}_{12}\}$ parameter planes. The stripe and plane-wave phases are denoted by black and white, respectively; dark (light) grey indicates the regions where the SP (PWP) is unstable. (a) Phase diagram for $\text{sgn}(g_1) = \tilde{g}_2 = 1$ and different values of $\tilde{g}_{12} = 0.1, 1, \text{ and } 2$. (b) Phase diagram for $\text{sgn}(g_1) = \tilde{g}_2 = -1$ and $\tilde{\Omega}_R = 0.1$.

phase begins to be unstable in the left bottom corner of this figure.

The magnetization $s_z = \tilde{k}_0 (2|c_1|^2 - 1)$ as a function of \tilde{U}_1 is illustrated with the black solid curve in Fig. 3 for $\text{sgn}(g_1) = \tilde{g}_2 = \delta\tilde{U} = 1$, $\tilde{g}_{12} = 2$, and $\tilde{\Omega}_R = 0.1$. For contrast, the magnetization when $\delta\tilde{U} = 0$ is also shown (blue dashed curve). Note that while the sign of the magnetization in the PWP is arbitrary for the $\delta\tilde{U} = 0$ case (a spontaneously broken symmetry in the ground state), in the present case the sign of s_z always follows that of $\delta\tilde{U}$. On the PWP side, the magnetization is fixed at its maximal value $s_z = \tilde{k}_0$; for $\tilde{U}_1 \gtrsim \tilde{U}_{1c}$ on the SP side, the magnetization decreases sharply before reaching an asymptotic value deep within the SP phase.

For small $\delta\tilde{U}$ and $\tilde{\Omega}_R$, the SP-PWP phase transition occurs at almost the same value of the critical cavity interaction $\tilde{U}_{1c}^0 = 0.5$ obtained using Eq. (13) which assumed $\delta\tilde{U} = 0$. Near the phase transition point on the SP side, one can write $c_1 = 1 - x^2$ and $c_2 = \sqrt{2}x$, where $x \ll 1$ and $c_1^2 + c_2^2 \simeq 1 + \mathcal{O}(x^4)$. Setting the term proportional to x^2 in $E_{\text{int}}[c_1 = 1, c_2 = 0] - E_{\text{int}}[c_1 = 1 - x^2, c_2 = \sqrt{2}x]$ equal to zero yields a modified critical cavity interaction

$$\tilde{U}_{1c} = \tilde{U}_{1c}^0 - \left[\frac{2 - (4 - \tilde{\Omega}_R^2)^{1/2} - \frac{1}{2}\tilde{\Omega}_R^2}{4 - \tilde{\Omega}_R^2} \right] \delta\tilde{U}. \quad (19)$$

In the small $\tilde{\Omega}_R$ limit this may be simplified to $\tilde{U}_{1c} \simeq \frac{1}{2}[\tilde{g}_{12} - \text{sgn}(g_1)] + \frac{1}{16}[\tilde{g}_{12} + \text{sgn}(g_1) + \delta\tilde{U}]\tilde{\Omega}_R^2$, which is the same critical cavity interaction \tilde{U}_{1c}^0 obtained above in the small $\tilde{\Omega}_R$ limit, save for the $\delta\tilde{U}$ -dependent correction.

The behavior of the magnetization for $\tilde{U}_1 > \tilde{U}_{1c}$ suggests that one can define the order parameter for the stripe phase to be $P = 1 - s_z/\tilde{k}_0 = 2(1 - c_1^2)$. As desired, this vanishes in the PWP (here we only consider a PWP with momentum $-\mathbf{k}_0$) and takes a nonzero value in SP. The order parameter is shown in the inset of Fig. 3. The

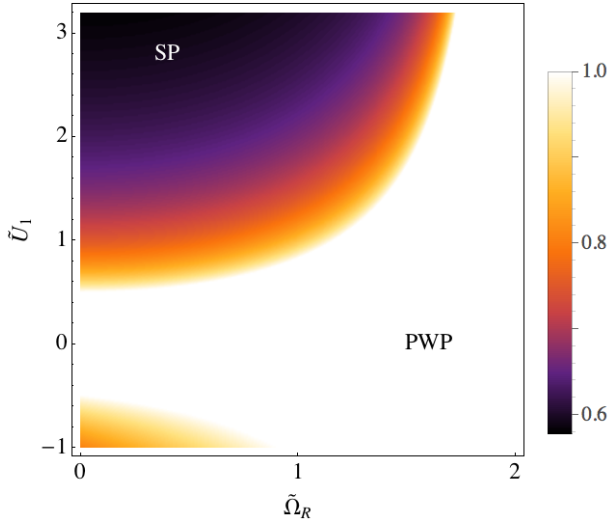


FIG. 2: (Color online) Density plot of $|c_1|^2$ in the $\{\tilde{U}_1, \tilde{\Omega}_R\}$ parameter plane for $\text{sgn}(g_1) = \tilde{g}_2 = \delta\tilde{U} = 1$, and $\tilde{g}_{12} = 2$. The plane-wave phase begins to be unstable in the left bottom corner.

discontinuity in the derivative of P with \tilde{U}_1 suggests that the SP-PWP quantum (zero-temperature) phase transition is second order. It is therefore of interest to determine the (mean-field) exponent β for the order parameter P in the vicinity of the transition point. Substituting $\tilde{U}_1 = \tilde{U}_{1c} + \chi$ into the energy functional E_{int} and minimizing it with respect to c_1 yields

$$c_1 = \sqrt{\frac{2\delta\tilde{U} (4 - \tilde{\Omega}_R^2)^{1/2} + \chi (4 - \tilde{\Omega}_R^2)}{2\delta\tilde{U} (4 - \tilde{\Omega}_R^2)^{1/2} + 2\chi (4 - \tilde{\Omega}_R^2)}}. \quad (20)$$

The order parameter $P = 2(1 - c_1^2)$ computed using this expression for c_1 is illustrated as the green dashed curve in the inset of Fig. 3, and is in excellent agreement with the numerical results of the variational approach, shown as the black solid curve. Taylor expanding c_1 in Eq. (20) for small χ and $\tilde{\Omega}_R$ up to first and second order, respectively, one obtains $c_1^{\text{MF}} \simeq 1 - \chi/2\delta\tilde{U}$ (the term proportional to $\chi\tilde{\Omega}_R^2$ is also omitted). This yields the mean-field order parameter $P_{\text{MF}} = 2\chi/\delta\tilde{U} = 2(\tilde{U}_1 - \tilde{U}_{1c})^\beta/\delta\tilde{U}$ and a critical exponent $\beta = 1$. The behavior of the order parameter near the transition point fits well to P , as is shown by the orange dashed curve in the inset of Fig. 3.

In principle, it is not valid to consider $\delta\tilde{U} \neq 0$ while at the same time assuming that $\tilde{\delta} \equiv \hbar\delta/E_R = 0$. Rather, if $\eta_1 \neq \eta_2 \neq 0$ but $\eta_1 \sim \eta_2$, then Eqs. (6) state that $\tilde{\delta} \sim \delta\tilde{U}$ whenever $\tilde{U}_1 \sim \tilde{\Omega}_R$. That said, in Fig. 3 the parameters are chosen so that $\tilde{\Omega}_R = 0.1 \ll \delta\tilde{U} = 1$. One can therefore expect $\tilde{\delta} \ll \delta\tilde{U}$ by a similar ratio, which again justifies neglecting it.

Consider briefly the effect of keeping a non-zero but small value of $\tilde{\delta}$. The single-particle dispersions of the

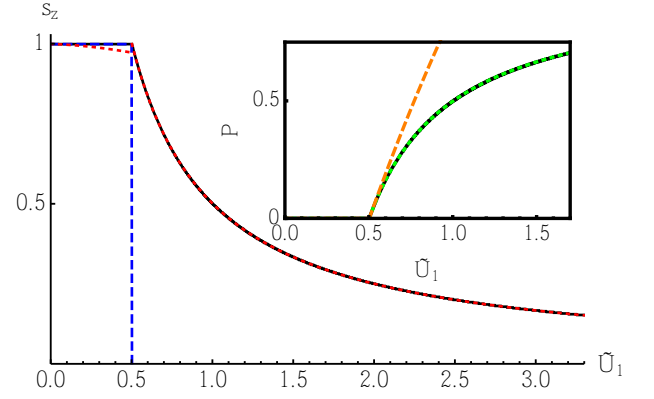


FIG. 3: (Color online) The magnetization s_z as a function of \tilde{U}_1 shown as the black solid curve for $\text{sgn}(g_1) = \tilde{g}_2 = \delta\tilde{U} = 1$, $\tilde{g}_{12} = 2$, and $\tilde{\Omega}_R = 0.1$. The blue dashed curve represents the magnetization when $\delta\tilde{U} = 0$. The red dotted curves are the magnetization computed from solutions of the coupled Gross-Pitaevskii equations in the SP and PWP assuming $\tilde{U}_{\text{ss}} = \tilde{U}_{\text{ds}} = \tilde{U}_1$ for the same parameters as the solid black curve, and $|g_1|\bar{n}/E_R = 1$. Inset: the SP order parameter P is shown as a function of \tilde{U}_1 (black curve); an analytical approximation (dashed green curve) and the behavior near the critical point (orange dashed curve) are shown for comparison.

spin-orbit Hamiltonian (4) become

$$\tilde{\epsilon}_\pm(\tilde{\mathbf{k}}) = \tilde{k}_z^2 + 1 \pm \sqrt{\frac{1}{4} (4\tilde{k}_z + \tilde{\delta})^2 + \tilde{\Omega}_R^2} \quad (21)$$

rather than the expressions given in Eq. (7a). The associated (orthogonal) eigenvectors have the same form as Eqs. (7b) but now $\sin 2\theta_{\mathbf{k}} = \tilde{\Omega}_R / \sqrt{\frac{1}{4} (4\tilde{k}_z + \tilde{\delta})^2 + \tilde{\Omega}_R^2}$. For $\tilde{\delta} \neq 0$, the lower double-well dispersion curve $\tilde{\epsilon}_-$ is no longer symmetric; rather, the right well is lower (higher) when $\tilde{\delta} > 0$ ($\tilde{\delta} < 0$). Thus, in the absence of particle interactions a PWP is energetically favored in one well or the other with no ambiguity. The presence of $\tilde{\delta}$ precludes a simple form like Eq. (8) for the location of the energy minima, but in the limit when both $\tilde{\Omega}_R \ll 1$ and $\tilde{\delta} \ll 1$ one obtains

$$\tilde{k}_0 \approx 1 - \frac{\tilde{\Omega}_R^2}{8} \left(1 - \frac{\tilde{\delta}}{2}\right). \quad (22)$$

The lowest-order contribution of $\tilde{\delta}$ is a correction to the coefficient of the already small $\tilde{\Omega}_R$ -dependent term, and therefore the value of \tilde{k}_0 is well-approximated by assuming $\tilde{\delta} = 0$. Likewise, the BEC approximation consists of \tilde{k}_z with \tilde{k}_0 ; because $4\tilde{k}_z \rightarrow 4\tilde{k}_0 \approx 4 \gg \tilde{\delta}$ in the expressions for the single-particle energies and eigenvectors above, $\tilde{\delta}$ can be similarly neglected in the calculations.

B. Coupled Gross-Pitaevskii Equations

While the variational calculation discussed in the previous section has revealed that a ring cavity can stabilize stripe phases in interacting spin-orbit coupled Bose-Einstein condensates, it is important to verify the results using a more rigorous approach. In this section, the coupled Gross-Pitaevskii (GP) equations are derived for both PWP and SP ansätze and the ground state properties are obtained from their solutions.

1. Plane wave phase

The GP equations can be obtained directly from the many-particle Hamiltonian (2):

$$\begin{aligned} & \left[\frac{\hbar^2}{2m} \hat{\Delta}_1 + g_1 |\psi_1|^2 + g_{12} |\psi_2|^2 + 2U_1 N_1 + 2U_{\text{ds}} S_x \right] \psi_1 \\ & + [\hbar\Omega_R + 2U_{\text{ss}} S_- + U_{\text{ds}} N] \psi_2 = \mu \psi_1, \\ & \left[\frac{\hbar^2}{2m} \hat{\Delta}_2 + g_2 |\psi_2|^2 + g_{12} |\psi_1|^2 + 2U_2 N_2 + 2U_{\text{ds}} S_x \right] \psi_2 \\ & + [\hbar\Omega_R + 2U_{\text{ss}} S_+ + U_{\text{ds}} N] \psi_1 = \mu \psi_2, \end{aligned} \quad (23)$$

where $\hat{\Delta}_1 = -\nabla_{\perp}^2 + (-i\partial_z + k_R)^2$ and $\hat{\Delta}_2 = -\nabla_{\perp}^2 + (-i\partial_z - k_R)^2$ and the BEC wavefunctions for the two spin components are denoted by $\psi_{1(2)}$ rather than $\psi_{1(2)}(\mathbf{r})$ to save space. These equations can be simplified in the plane-wave phase by assuming homogeneous wavefunctions $\psi_{\tau}(\mathbf{r}) = e^{\pm ik_0 z} \bar{\psi}_{\tau}$, where the upper (lower) sign corresponds to a condensate in the right (left) minimum. The GP equations are then recast as

$$\begin{aligned} & [\tilde{\mu} - (\tilde{k}_0 \pm 1)^2] \bar{\psi}_1 - \tilde{\Omega}_R \bar{\psi}_2 \\ & = \frac{|g_1|}{E_R} \left\{ \left[(\text{sgn}(g_1) + 2\tilde{U}_1) |\bar{\psi}_1|^2 + (\tilde{g}_{12} + 2\tilde{U}_{\text{ss}}) |\bar{\psi}_2|^2 \right] \bar{\psi}_1 \right. \\ & \left. + \tilde{U}_{\text{ds}} (2|\bar{\psi}_1|^2 + |\bar{\psi}_2|^2) \bar{\psi}_2 + \tilde{U}_{\text{ds}} \bar{\psi}_1^2 \bar{\psi}_2^* \right\}; \\ & [\tilde{\mu} - (\tilde{k}_0 \mp 1)^2] \bar{\psi}_2 - \tilde{\Omega}_R \bar{\psi}_1 \\ & = \frac{|g_1|}{E_R} \left\{ \left[(\tilde{g}_2 + 2\tilde{U}_2) |\bar{\psi}_2|^2 + (\tilde{g}_{12} + 2\tilde{U}_{\text{ss}}) |\bar{\psi}_1|^2 \right] \bar{\psi}_2 \right. \\ & \left. + \tilde{U}_{\text{ds}} (|\bar{\psi}_1|^2 + 2|\bar{\psi}_2|^2) \bar{\psi}_1 + \tilde{U}_{\text{ds}} \bar{\psi}_2^2 \bar{\psi}_1^* \right\}, \end{aligned} \quad (24)$$

where again the upper (lower) sign in each equation corresponds to a condensate in the right (left) minimum, and the chemical potential is expressed in recoil energy units, $\tilde{\mu} \equiv \mu/E_R$.

The chemical potential can be obtained from the first of Eqs. (24) and then substituted into the second. Under the assumption that both condensate wavefunctions are

real, $\tilde{U}_1 = \tilde{U}_{\text{ss}} = \tilde{U}_{\text{ds}}$, and $\text{sgn}(g_1) = \tilde{g}_2$, one obtains

$$\begin{aligned} & \frac{|g_1|}{E_R} \left[(\tilde{g}_{12} - \text{sgn}(g_1)) (\bar{\psi}_2^2 - \bar{\psi}_1^2) \bar{\psi}_1 \bar{\psi}_2 + \tilde{U}_1 (\bar{\psi}_2^4 - \bar{\psi}_1^4) \right] \\ & \pm 4\tilde{k}_0 \bar{\psi}_1 \bar{\psi}_2 + \tilde{\Omega}_R (\bar{\psi}_2^2 - \bar{\psi}_1^2) = 0. \end{aligned} \quad (25)$$

For the plane-wave phase, both $\bar{\psi}_1$ and $\bar{\psi}_2$ are assumed to be constant, so that $\bar{\psi}_1^2 + \bar{\psi}_2^2 = \bar{n}$ and $\bar{\psi}_1^2 - \bar{\psi}_2^2 = \bar{n} s_z$. Inserting these into Eq. (25) gives

$$\begin{aligned} & \sqrt{1 - s_z^2} \left[\mp 4\tilde{k}_0 + s_z \frac{|g_1| \bar{n}}{E_R} (\tilde{g}_{12} - \text{sgn}(g_1)) \right] \\ & + 2s_z \left(\tilde{\Omega}_R + \tilde{U}_1 \frac{|g_1| \bar{n}}{E_R} \right) = 0. \end{aligned} \quad (26)$$

When $\tilde{U}_1 = 0$ and $\tilde{\Omega}_R \approx 0$, this expression is approximately correct when $s_z \approx 1$, consistent with the variational results in this regime. Recall that in the variational approach, the magnetization $s_z = \tilde{k}_0$ is constant [c.f. Eq. (11)], solely determined by $\tilde{\Omega}_R$. Unlike the variational result, however, it is immediately apparent from the second term in Eq. (26) that the magnetization must decrease monotonically as \tilde{U}_1 is increased.

The magnetization s_z obtained via numerical solution of Eq. (26) is shown as the red dotted curve in Fig. 3 for a condensate in the left well (i.e. choosing the lower sign) of the PWP for $\tilde{U}_1 \leq \tilde{U}_{1c}$. Parameters are $\tilde{U}_1 = \tilde{U}_{\text{ss}} = \tilde{U}_{\text{ds}}$, $\text{sgn}(g_1) = \tilde{g}_2 = |g_1| \bar{n} / E_R = \delta \tilde{U} = 1$, $\tilde{g}_{12} = 2$, and $\tilde{\Omega}_R = 0.1$. As expected, the magnetization decreases monotonically with \tilde{U}_1 from its maximum at $\tilde{U}_1 = 0$. The difference between the results of the two methods has its origins in the fact that the variational ansatz, Eq. (9), is a single-particle wavefunction which satisfies the GP equations in PWP only when all the two-body and cavity-mediated interactions are zero. In principle, the variational ansatz could be remedied by allowing both k_0 and $\theta_{\mathbf{k}_0}$ to be variational parameters [12]. The dependence of the solution of GP equations on the two-body and cavity-mediated interactions will be investigated further in Sec. III C 1 in the calculation of the elementary excitations in the PWP.

2. Stripe phase

The momentum dependence of the condensate in the SP is not as readily apparent as it is for the PWP. It is therefore convenient to instead construct an effective low energy Hamiltonian by first mapping the complete Hamiltonian (2) into the lower band and then deriving the low energy coupled GP equations [14, 34]. This is reasonable because the occupation of the upper band $\epsilon_+(\mathbf{k})$ can be assumed to be small at low temperatures $k_B T \ll \hbar\Omega_R$. Furthermore, only states in the vicinity of the two minima $\pm \mathbf{k}_0$ will be occupied.

The field operators $\tilde{\Psi}(\mathbf{r})$ can then be expanded in the lower band basis around the two minima (recall that

$\phi_-(\mathbf{k})$ is the *two-component* spinor in the lower band):

$$\hat{\Psi}(\mathbf{r}) \simeq \sum_{\mathbf{q} < \mathbf{q}_c} \left[e^{i(-\mathbf{k}_0 + \mathbf{q}) \cdot \mathbf{r}} \phi_-(-\mathbf{k}_0 + \mathbf{q}) \hat{\varphi}_-(-\mathbf{k}_0 + \mathbf{q}) + e^{i(\mathbf{k}_0 + \mathbf{q}) \cdot \mathbf{r}} \phi_-(\mathbf{k}_0 + \mathbf{q}) \hat{\varphi}_-(\mathbf{k}_0 + \mathbf{q}) \right], \quad (27)$$

where the sum over \mathbf{q} need only be taken up to some maximum \mathbf{q}_c . Approximating the spinor $\phi_-(\pm\mathbf{k}_0 + \mathbf{q}) \simeq \phi_-(\pm\mathbf{k}_0)$ in the limit $\tilde{\Omega}_R \ll 2$ and defining the new operators $\hat{\varphi}_{1'}(\mathbf{q}) \equiv \hat{\varphi}_-(-\mathbf{k}_0 + \mathbf{q})$ and $\hat{\varphi}_{2'}(\mathbf{q}) \equiv \hat{\varphi}_-(\mathbf{k}_0 + \mathbf{q})$ [14], the field operators read

$$\hat{\Psi}(\mathbf{r}) = e^{-i\mathbf{k}_0 \cdot \mathbf{r}} \phi_-(-\mathbf{k}_0) \hat{\psi}_{1'}(\mathbf{r}) + e^{i\mathbf{k}_0 \cdot \mathbf{r}} \phi_-(\mathbf{k}_0) \hat{\psi}_{2'}(\mathbf{r}), \quad (28)$$

where $\hat{\psi}_{\tau'}(\mathbf{r}) = \sum_{\mathbf{q}} e^{i\mathbf{q} \cdot \mathbf{r}} \hat{\varphi}_{\tau'}(\mathbf{q})$. In the small $\tilde{\Omega}_R$ limit and keeping terms only up to second order in $\tilde{\Omega}_R$ and noting that $k_0 \simeq (1 - \tilde{\Omega}_R^2/8)k_R$, the field operators can be further simplified to

$$\begin{bmatrix} \hat{\psi}_{1'}(\mathbf{r}) \\ \hat{\psi}_{2'}(\mathbf{r}) \end{bmatrix} \simeq \begin{bmatrix} (1 - \frac{\tilde{\Omega}_R^2}{32})e^{-ik_0z} & \frac{\tilde{\Omega}_R}{4}e^{ik_0z} \\ -\frac{\tilde{\Omega}_R}{4}e^{-ik_0z} & -(1 - \frac{\tilde{\Omega}_R^2}{32})e^{ik_0z} \end{bmatrix} \begin{bmatrix} \hat{\psi}_{1'}(\mathbf{r}) \\ \hat{\psi}_{2'}(\mathbf{r}) \end{bmatrix}. \quad (29)$$

Note that the lab-frame pseudospin field operator $\hat{\psi}_\tau$ maps correctly to the corresponding dressed pseudospin field operator $\hat{\psi}_{\tau'}$ in the $\tilde{\Omega}_R \rightarrow 0$ limit; recall that $\hat{\Psi}(\mathbf{r}) = \mathcal{Q}_2^\dagger \hat{\Psi}(\mathbf{r})$. Substituting Eq. (29) back into the original Hamiltonian (2) and only keeping terms to second order in $\tilde{\Omega}_R$ yields the effective low-energy Hamiltonian:

$$H_e = \int d^3r \left(\hat{\Psi}^\dagger H_e^{(1)} \hat{\Psi}' + \frac{1}{2}g'_1 \hat{n}_{1'}^2 + \frac{1}{2}g'_2 \hat{n}_{2'}^2 + g'_{12} \hat{n}_{1'} \hat{n}_{2'} \right) + \frac{1}{2}U'_1 \hat{N}_{1'}^2 + \frac{1}{2}U'_2 \hat{N}_{2'}^2 + U'_{12} \hat{N}_{1'} \hat{N}_{2'}, \quad (30)$$

where $\hat{\Psi}'(\mathbf{r}) = (\hat{\psi}_{1'}(\mathbf{r}), \hat{\psi}_{2'}(\mathbf{r}))^\top$, as before $\hat{N}_{\tau'} = \int \hat{n}_{\tau'}(\mathbf{r}) d^3r = \int \hat{\psi}_{\tau'}^\dagger(\mathbf{r}) \hat{\psi}_{\tau'}(\mathbf{r}) d^3r$ is the total atomic number operator for the dressed pseudospin $\tau' \in \{1', 2'\}$, and we have introduced the dressed interaction parameters

$$\begin{aligned} g'_\tau &\equiv g_{\tau'\tau'} = g_\tau - \frac{1}{8}(g_\tau - g_{12})\tilde{\Omega}_R^2, \\ g'_{12} &\equiv g_{1'2'} = g_{12} + \frac{1}{8}(g_1 + g_2)\tilde{\Omega}_R^2, \\ U'_\tau &\equiv U_{\tau'\tau'} = 2U_\tau - U_{\text{ds}}\tilde{\Omega}_R - \frac{1}{4}(U_\tau - U_{\text{ss}})\tilde{\Omega}_R^2, \\ U'_{12} &\equiv U_{1'2'} = -U_{\text{ds}}\tilde{\Omega}_R + \frac{1}{8}(U_1 + U_2 + 2U_{\text{ss}})\tilde{\Omega}_R^2, \end{aligned} \quad (31)$$

with $\tau \in \{1, 2\}$ and $\tau' \in \{1', 2'\}$.

The single-particle part of the effective low energy Hamiltonian $H_e^{(1)} = (-\hbar^2/2m)[\nabla_\perp^2 + (1 - \tilde{\Omega}_R^2/4)\partial_z^2]$ can be easily diagonalized [14], yielding the effective low energy

dispersion $\epsilon_e(\mathbf{k})/E_R = \tilde{k}_\perp^2 + (1 - \tilde{\Omega}_R^2/4)\tilde{k}_z^2$. It is important to note that the lowest single-particle energy state for both dressed pseudospins is the $\mathbf{k} = 0$ momentum state, not $\mathbf{k} = \pm\mathbf{k}_0$ as it was for the actual pseudospins. Then the effective low energy GP equations for the SP can be obtained from H_e , Eq. (30):

$$\begin{aligned} \left[(\tilde{g}'_1 + \tilde{U}'_1) |\psi_{1'}|^2 + (\tilde{g}'_{12} + \tilde{U}'_{12}) |\psi_{2'}|^2 \right] \psi_{1'} &= \bar{\mu} \psi_{1'}, \\ \left[(\tilde{g}'_2 + \tilde{U}'_2) |\psi_{2'}|^2 + (\tilde{g}'_{12} + \tilde{U}'_{12}) |\psi_{1'}|^2 \right] \psi_{2'} &= \bar{\mu} \psi_{2'}, \end{aligned} \quad (32)$$

where the dressed pseudospin wavefunctions $\psi_{\tau'}$ are assumed to be homogeneous and unitless parameters have been introduced for convenience: $\tilde{g}'_\tau = g'_\tau/|g_1|$, $\tilde{g}'_{12} = g'_{12}/|g_1|$, $\tilde{U}'_\tau = VU'_\tau/|g_1|$, and $\tilde{U}'_{12} = VU'_{12}/|g_1|$. Here $\bar{\mu} = \mu/|g_1|$ which has units of inverse volume. These algebraic equations have the solution

$$\begin{aligned} n_{1'} &= \frac{2\tilde{U}'_2 + \tilde{g}'_2 - \tilde{g}'_{12} - \frac{1}{8}(\tilde{U}'_1 + 3\tilde{U}'_2)\tilde{\Omega}_R^2}{\tilde{g}'_1 + \tilde{g}'_2 - 2\tilde{g}'_{12} + 2(\tilde{U}'_1 + \tilde{U}'_2)\left(1 - \frac{1}{4}\tilde{\Omega}_R^2\right)} \bar{n}, \\ n_{2'} &= \frac{2\tilde{U}'_1 + \tilde{g}'_1 - \tilde{g}'_{12} - \frac{1}{8}(3\tilde{U}'_1 + \tilde{U}'_2)\tilde{\Omega}_R^2}{\tilde{g}'_1 + \tilde{g}'_2 - 2\tilde{g}'_{12} + 2(\tilde{U}'_1 + \tilde{U}'_2)\left(1 - \frac{1}{4}\tilde{\Omega}_R^2\right)} \bar{n}, \end{aligned} \quad (33)$$

where $n_{1'} + n_{2'} = \bar{n}$. Note that although the GP equations for the SP, Eq. (32), depend on the cavity parameters \tilde{U}_{ss} and \tilde{U}_{ds} , these solutions do not; rather, \tilde{U}'_1 and \tilde{U}'_2 are the only cavity interaction parameters that affect $\psi_{\tau'}$, consistent with the variational approach of Sec. III A.

The dressed magnetization $s'_z = (n_{1'} - n_{2'})/\bar{n}$ can easily be obtained from Eq. (33), and the actual magnetization $s_z = s'_z(1 - \tilde{\Omega}_R^2/8)$ up to $\mathcal{O}(\tilde{\Omega}_R^3)$ is found using Eq. (29):

$$s_z = \frac{[\tilde{g}'_2 - \tilde{g}'_1 + 2\delta\tilde{U}\left(1 - \frac{1}{8}\tilde{\Omega}_R^2\right)]\left(1 - \frac{1}{8}\tilde{\Omega}_R^2\right)}{\tilde{g}'_1 + \tilde{g}'_2 - 2\tilde{g}'_{12} + 2(\tilde{U}'_1 + \tilde{U}'_2)\left(1 - \frac{1}{4}\tilde{\Omega}_R^2\right)}. \quad (34)$$

The SP magnetization s_z is displayed as a function of $\tilde{U}'_1 (\geq \tilde{U}'_{1c})$ in Fig. 3 with the red dotted curve for $\text{sgn}(g_1) = \tilde{g}_2 = \delta\tilde{U} = 1$, $\tilde{g}_{12} = 2$, and $\tilde{\Omega}_R = 0.1$. The behavior is indistinguishable from the magnetization obtained from the variational approach, Eq. (11). The critical cavity interaction for the SP-PWP phase transition can be obtained from Eq. (33) by setting $n_{1'} = \bar{n}$ (or setting $s'_z = 1$):

$$\begin{aligned} \tilde{U}'_{1c} = \frac{1}{4(4 - \tilde{\Omega}_R^2)} \left\{ - \left[\tilde{g}_{12} - \text{sgn}(g_1) - 2\tilde{g}_2 - \delta\tilde{U} \right] \tilde{\Omega}_R^2 \right. \\ \left. + 8[\tilde{g}_{12} - \text{sgn}(g_1)] \right\}, \end{aligned} \quad (35)$$

for a phase transition from SP to a PWP at the left minimum. Instead setting $n_{1'} = 0$ (or $s'_z = -1$) for a phase

transition from SP to a PWP at the right minimum, one obtains

$$\tilde{U}_{1c}^R = \frac{1}{4(4 - \tilde{\Omega}_R^2)} \left\{ - \left[\tilde{g}_{12} - \text{sgn}(g_1) - 2\tilde{g}_2 - 3\delta\tilde{U} \right] \tilde{\Omega}_R^2 + 8 \left[\tilde{g}_{12} - \text{sgn}(g_1) - 2\delta\tilde{U} \right] \right\}. \quad (36)$$

Note that when $\text{sgn}(g_1) = \tilde{g}_2$ and $\delta\tilde{U} = 0$, the two critical cavity interactions \tilde{U}_{1c}^L and \tilde{U}_{1c}^R become equal to the value \tilde{U}_{1c}^0 found using the variational approach, Eq. (13).

C. Elementary Excitations: Bogoliubov theory

Thus far we have treated the bosons as classical fields, having replaced the field operators with their expectation values $\hat{\psi}_\tau \rightarrow \psi_\tau \equiv \langle \hat{\psi}_\tau \rangle$. In this section, we consider the quantum fluctuations of the fields and obtain the elementary excitation spectrum using Bogoliubov theory. This is accomplished by writing the field operators as $\hat{\psi}_\tau = \psi_\tau + \delta\hat{\psi}_\tau$, where $\delta\hat{\psi}_\tau$ is the quantum fluctuation operator. These expressions are substituted into the time-dependent GP equations and the resulting equations are linearized, i.e. terms are retained only up to first order in the fluctuations. One then obtains a set of time-dependent coupled equations for $\delta\hat{\psi}_\tau$ which yields, after diagonalization, the elementary excitation spectrum.

1. Plane wave phase

Following the approach taken in Sec. III B 1 for the PWP, it is reasonable to define the bosonic field operator

$$\hat{\psi}_\tau(\mathbf{r}, t) \equiv e^{\pm ik_0 z} \left[\bar{\psi}_\tau + \delta\hat{\psi}_\tau(\mathbf{r}, t) \right], \quad (37)$$

where $\bar{\psi}_\tau$ are the time-independent, homogeneous solutions of the coupled GP equations (24) in the PWP. To consider time-dependent fluctuations around the equilibrium solutions it is convenient to replace the chemical potential (which is the eigenvalue of the time-independent GP equations) by a time-dependent operator, $\mu \rightarrow \mu + i\hbar\partial_t$. The time-dependent fluctuations can then be expressed using the usual Bogoliubov approach in terms of particle and hole excitations with amplitudes $\bar{u}_{\tau,\mathbf{q}} e^{i(\mathbf{q}\cdot\mathbf{r} - \omega t)}$ and $\bar{v}_{\tau,\mathbf{q}}^* e^{-i(\mathbf{q}\cdot\mathbf{r} - \omega t)}$, respectively.

Consider the specific case of a condensate in the left minimum $-\tilde{\mathbf{k}}_0$ of the double-well single-particle dispersion relation; for condensation in the right well one need only replace \tilde{k}_0 in what follows with $-\tilde{k}_0$. Substituting Eq. (37) into the time-dependent GP equations and keeping only linear terms in the fluctuations, one obtains the following non-Hermitian eigenvalue equation for each value of \mathbf{q} :

$$\begin{pmatrix} M_{11} & g_1 \bar{\psi}_1^2 & g_{12} \bar{\psi}_1 \bar{\psi}_2^* + \hbar\Omega_{\text{eff}} & g_{12} \bar{\psi}_1 \bar{\psi}_2 \\ -g_1 \bar{\psi}_1^{*2} & -M_{22} & -g_{12} \bar{\psi}_1^* \bar{\psi}_2^* & -g_{12} \bar{\psi}_1^* \bar{\psi}_2 - \hbar\Omega_{\text{eff}}^* \\ g_{12} \bar{\psi}_1^* \bar{\psi}_2 + \hbar\Omega_{\text{eff}}^* & g_{12} \bar{\psi}_1 \bar{\psi}_2 & M_{33} & g_2 \bar{\psi}_2^2 \\ -g_{12} \bar{\psi}_1^* \bar{\psi}_2^* & -g_{12} \bar{\psi}_1 \bar{\psi}_2^* - \hbar\Omega_{\text{eff}} & -g_2 \bar{\psi}_2^{*2} & -M_{44} \end{pmatrix} \begin{pmatrix} \bar{u}_{1,\mathbf{q}} \\ \bar{v}_{1,\mathbf{q}} \\ \bar{u}_{2,\mathbf{q}} \\ \bar{v}_{2,\mathbf{q}} \end{pmatrix} = \hbar\omega(\mathbf{q}) \begin{pmatrix} \bar{u}_{1,\mathbf{q}} \\ \bar{v}_{1,\mathbf{q}} \\ \bar{u}_{2,\mathbf{q}} \\ \bar{v}_{2,\mathbf{q}} \end{pmatrix}, \quad (38)$$

where

$$\begin{aligned} M_{11/22} &= E_R \left[\tilde{q}^2 \mp 2(\tilde{k}_0 - 1)\tilde{q}_z \right] + g_1 |\bar{\psi}_1|^2 - \hbar\Omega_{\text{eff}} \frac{\bar{\psi}_2}{\bar{\psi}_1}, \\ M_{33/44} &= E_R \left[\tilde{q}^2 \mp 2(\tilde{k}_0 + 1)\tilde{q}_z \right] + g_2 |\bar{\psi}_2|^2 - \hbar\Omega_{\text{eff}}^* \frac{\bar{\psi}_1}{\bar{\psi}_2}, \\ \hbar\Omega_{\text{eff}} &= \hbar\Omega_R + |g_1| |\tilde{U}_{\text{ds}} \bar{n} + 2|g_1| \tilde{U}_{\text{ss}} \bar{\psi}_1 \bar{\psi}_2^*. \end{aligned} \quad (39)$$

In deriving the Bogoliubov Hamiltonian (38), we made use of the fact that $\hat{N}_\tau = \int \hat{\psi}_\tau^\dagger(\mathbf{r}, t) \hat{\psi}_\tau(\mathbf{r}, t) d\mathbf{r} = \int |\bar{\psi}_\tau|^2 d\mathbf{r} = V |\bar{\psi}_\tau|^2 = N_\tau$, because $\bar{\psi}_\tau$ is homogeneous by assumption and $\int \delta\hat{\psi}_\tau(\mathbf{r}, t) d\mathbf{r} = 0$ because the spatial integral of either Bogoliubov amplitude $\bar{u}_{\tau,\mathbf{q}} e^{i(\mathbf{q}\cdot\mathbf{r} - \omega t)}$ or $\bar{v}_{\tau,\mathbf{q}}^* e^{-i(\mathbf{q}\cdot\mathbf{r} - \omega t)}$ is zero for any $\mathbf{q} \neq 0$. A similar argument ensures that $\hat{S}_+ = S_+$ and $\hat{S}_- = S_-$ as well. Note also that the chemical potential in Eq. (38) has been eliminated using the coupled GP equations (24).

Diagonalizing Eq. (38) yields the spectrum $\omega_\pm^{\text{PW}}(\mathbf{q})$ of collective excitations. The results are shown in Fig. 4(a) for the parameters $\text{sgn}(g_1) = \tilde{g}_2 = |g_1| \bar{n} / E_R = 1$, $\tilde{g}_{12} = 2$, and $\tilde{\Omega}_R = 0.1$, when all the cavity-mediated interaction terms are zero ($\tilde{U}_1 = \tilde{U}_2 = \tilde{U}_{\text{ss}} = \tilde{U}_{\text{ds}} = 0$), i.e. the system is deep in the PWP. The lower curve exhibits the usual superfluid sound-like linear dispersion around the origin $\tilde{q}_z \equiv q_z / k_R = 0$ (around the left minimum of the single-particle energy dispersion where all the atoms are condensed) and a roton-type minimum around $\tilde{q}_z \simeq 2$. As the cavity interactions are increased, the energy of the roton minimum lowers. For parameters $\tilde{U}_1 = 0.5$, $\delta\tilde{U} = 1.5$, $\tilde{U}_{\text{ss}} = \tilde{U}_{\text{ds}} = 0$, and the other parameters same as in Fig. 4(a), this minimum coincides with zero energy (i.e. the excitation energy at the origin $\tilde{q}_z = 0$); see the black solid curve in Fig. 4(b). The red dashed-dotted curve represents the elementary excitation spectrum for the same values of \tilde{U}_1 and $\delta\tilde{U}$ but

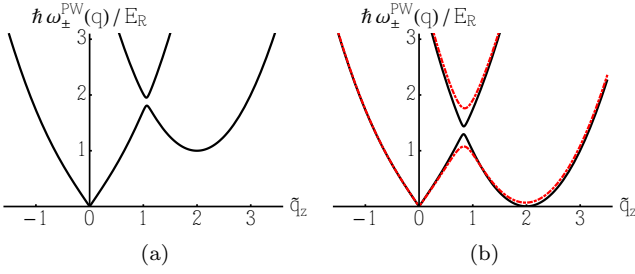


FIG. 4: (Color online) Elementary excitation spectrum in the PWP for $\text{sgn}(g_1) = \tilde{g}_2 = |g_1|\bar{n}/E_R = 1$, $\tilde{g}_{12} = 2$, and $\tilde{\Omega}_R = 0.1$. $(\tilde{U}_1, \tilde{U}_2, \tilde{U}_{\text{ss}}, \tilde{U}_{\text{ds}}) = (0, 0, 0, 0)$ in (a), and $(0.5, 1.5, 0, 0)$ and $(0.5, 1.5, 0.5, 0.5)$ in (b) for the black solid and red dashed-dotted curves, respectively.

for $\tilde{U}_{\text{ss}} = \tilde{U}_{\text{ds}} = 0.5$. In this case, $\hbar\Omega_{\text{eff}}/E_R$ [cf. Eq. (39)] is somewhat bigger than the bare $\tilde{\Omega}_R = 0.1$ for the black solid curve, so the roton minimum lies somewhat above that of the black solid curve around $\tilde{q}_z \simeq 2$.

The energy of the roton minimum near $q_z \simeq 2k_R$ can be reduced below zero by further increasing the cavity interaction strength \tilde{U}_1 . This signals a dynamic instability toward the formation of the SP; recall from Eq. (10) that the density modulation in the SP has wave vector $2k_0 \simeq 2k_R$ for $\tilde{\Omega}_R \rightarrow 0$. The critical cavity interactions for the black solid and the red dashed-dotted excitation spectra in Fig. 4(b) are $\tilde{U}_{1c} \simeq 0.5$ and 0.53 , respectively,

and these are in good agreement with that of the variational approach, where Eq. (19) predicts a phase transition between the PWP and the SP at the critical value $\tilde{U}_{1c} \simeq 0.5$ for the parameters $\text{sgn}(g_1) = \tilde{g}_2 = \delta\tilde{U} = 1$, $\tilde{g}_{12} = 2$, and $\tilde{\Omega}_R = 0.1$ (cf. also Fig. 3).

If one hypothetically sets $\tilde{U}_{\text{ss}} = \tilde{U}_{\text{ds}} = 0$ in the PWP, then the critical cavity interaction \tilde{U}_{1c} obtained from the analysis of the elementary excitations and the variational method would match exactly with each other for any range of parameters. Nevertheless, they begin to deviate from one another as \tilde{U}_{ss} and \tilde{U}_{ds} become larger and larger, because Eq. (19) is independent of these cavity interaction parameters while both the coupled GP equations and the Bogoliubov Hamiltonian depend explicitly on them (the latter through $\hbar\Omega_{\text{eff}}$). That said, we have compared the critical phase transition point \tilde{U}_{1c} obtained from both the variational approach and the elementary excitation spectrum in the PWP and have found that when $\tilde{U}_1 = \tilde{U}_{\text{ss}} = \tilde{U}_{\text{ds}}$ they agree with one another within a $\sim 8\%$ error for \tilde{g}_{12} in the range of $\sim 0 - 8$, assuming $\text{sgn}(g_1) = \tilde{g}_2 = |g_1|\bar{n}/E_R = \delta\tilde{U} = 1$ and $\tilde{\Omega}_R = 0.1$.

2. Stripe phase

The derivation of the Bogoliubov excitation spectrum begins with the corresponding time-dependent, effective low energy GP equations in the SP [c.f. Eq. (32)]:

$$\begin{aligned} i\hbar \frac{\partial}{\partial t} \hat{\psi}_{1'} &= \left(H_e^{(1)} + g'_1 |\hat{\psi}_{1'}|^2 + g'_{12} |\hat{\psi}_{2'}|^2 + U'_1 \hat{N}_{1'} + U'_{12} \hat{N}_{2'} - \mu \right) \hat{\psi}_{1'}, \\ i\hbar \frac{\partial}{\partial t} \hat{\psi}_{2'} &= \left(H_e^{(1)} + g'_2 |\hat{\psi}_{2'}|^2 + g'_{12} |\hat{\psi}_{1'}|^2 + U'_2 \hat{N}_{2'} + U'_{12} \hat{N}_{1'} - \mu \right) \hat{\psi}_{2'}. \end{aligned} \quad (40)$$

As in the PWP case, the low energy field operators are replaced with $\hat{\psi}_{\tau'}(\mathbf{r}, t) = \psi_{\tau'} + \delta\hat{\psi}_{\tau'}(\mathbf{r}, t)$ in these equations. Here $\psi_{\tau'}$ are the time-independent, homogeneous solutions of the effective low energy GP equations in the SP, Eq. (33), and $\delta\hat{\psi}_{\tau'}(\mathbf{r}, t)$ are the quantum fluctuations. Linearizing Eq. (40) yields the Bogoliubov Hamiltonian:

$$\begin{pmatrix} \epsilon_e(\mathbf{q}) + g'_1 |\psi_{1'}|^2 & g'_1 \psi_{1'}^2 & g'_{12} \psi_{1'} \psi_{2'}^* & g'_{12} \psi_{1'} \psi_{2'} \\ -g'_1 \psi_{1'}^{*2} & -\epsilon_e(\mathbf{q}) - g'_1 |\psi_{1'}|^2 & -g'_{12} \psi_{1'}^* \psi_{2'}^* & -g'_{12} \psi_{1'}^* \psi_{2'} \\ g'_{12} \psi_{1'}^* \psi_{2'} & g'_{12} \psi_{1'} \psi_{2'} & \epsilon_e(\mathbf{q}) + g'_2 |\psi_{2'}|^2 & g'_2 \psi_{2'}^2 \\ -g'_{12} \psi_{1'}^* \psi_{2'}^* & -g'_{12} \psi_{1'} \psi_{2'}^* & -g'_2 \psi_{2'}^{*2} & -\epsilon_e(\mathbf{q}) - g'_2 |\psi_{2'}|^2 \end{pmatrix} \begin{pmatrix} u_{1',\mathbf{q}} \\ v_{1',\mathbf{q}} \\ u_{2',\mathbf{q}} \\ v_{2',\mathbf{q}} \end{pmatrix} = \hbar\omega(\mathbf{q}) \begin{pmatrix} u_{1',\mathbf{q}} \\ v_{1',\mathbf{q}} \\ u_{2',\mathbf{q}} \\ v_{2',\mathbf{q}} \end{pmatrix}, \quad (41)$$

which can be diagonalized to give the spectrum of the elementary excitations:

$$\hbar\omega_{\pm}^{\text{SP}}(\mathbf{q}) = \sqrt{\epsilon_e^2(\mathbf{q}) + \epsilon_e(\mathbf{q}) \left(D_1 \pm \sqrt{D_1^2 - 4D_2} \right)}, \quad (42)$$

with

$$\begin{aligned} D_1 &= g'_1 n_{1'} + g'_2 n_{2'}, \\ D_2 &= (g'_1 g'_2 - g'^2_{12}) n_{1'} n_{2'}. \end{aligned} \quad (43)$$

We have again used the fact that $\hat{N}_{\tau'} = N_{\tau'}$.

Surprisingly, the Bogoliubov Hamiltonian in the SP does not depend explicitly on the cavity parameters and the form of the excitation spectrum coincides with the

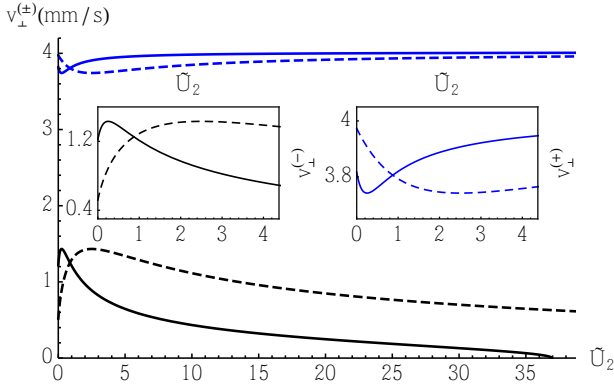


FIG. 5: (Color online) The speed of sound in the transverse direction $v_{\perp}^{(\pm)}$ is shown as a function of \tilde{U}_2 for $\tilde{U}_1 = 1/4$ (solid curves) and $\tilde{U}_1 = 5/2$ (dashed curves). For all curves: $\tilde{\Omega}_R = 0.4$, $\text{sgn}(g_1) = \tilde{g}_2 = 1$, $\tilde{g}_{12} = 0.7$, $g_1 \bar{n}/E_R = 1$, and m is the mass of ^{87}Rb atom. The insets show the results closer to the origin.

quasiparticle spectrum of a Raman-induced stripe phase BEC [14]. That said, the excitation spectrum implicitly depends on the cavity parameters \tilde{U}'_{τ} through $n_{\tau'}$, as can be seen in Eq. (33). Both $\omega_{\pm}^{\text{SP}}(\mathbf{q})$ are gapless and exhibit linear dispersion at long wavelengths, the characteristic of superfluidity in this phase; the slope of the dispersion relation at long wavelength corresponds to the speed of sound in the medium. In the transverse direction, one obtains

$$v_{\perp}^{(\pm)} = \left. \frac{d\omega_{\pm}^{\text{SP}}(\mathbf{q})}{dq_{\perp}} \right|_{\mathbf{q} \rightarrow 0} = \frac{1}{\sqrt{2m}} \sqrt{D_1 \pm \sqrt{D_1^2 - 4D_2}}, \quad (44)$$

and the speed of sound in the z (SO-coupling) direction is nearly the same for small $\tilde{\Omega}$, $v_z^{(\pm)} = v_{\perp}^{(\pm)} \sqrt{1 - \tilde{\Omega}_R^2/4}$.

Figure 5 depicts $v_{\perp}^{(\pm)}$ as a function of \tilde{U}_2 for $\tilde{U}_1 = 1/4$ (solid curves) and $\tilde{U}_1 = 5/2$ (dashed curves), with the other parameters fixed to $\text{sgn}(g_1) = \tilde{g}_2 = 1$, $\tilde{g}_{12} = 0.7$, $\tilde{\Omega}_R = 0.4$, and $g_1 \bar{n}/E_R = 1$. The mass is assumed to be that of ^{87}Rb . As \tilde{U}_2 is increased above zero, the speed of sound in the positive branch $v_{\perp}^{(+)}$ (the blue curves) first decreases quickly and reaches a minimum around $\delta\tilde{U} = \tilde{U}_2 - \tilde{U}_1 \sim 0$ for both curves, and then gradually approaches its asymptotic value. The speed of sound in the negative branch $v_{\perp}^{(-)}$ (black curves) has the opposite behavior, first increasing sharply to a maximum again near $\delta\tilde{U} \sim 0$ for both curves, before asymptotically approaching zero. The insets show the behaviour of $v_{\perp}^{(\pm)}$ close to the origin. The asymptotic behaviour of the speed of sound can be understood by noting that for large positive $\tilde{U}_2 \gg \tilde{U}_1$, $n_{1'}$ approaches \bar{n} and $n_{2'}$ approaches zero [c.f. Eqs. (33)]. As a consequence $D_2 \rightarrow 0$ and $v_{\perp}^{(-)} \rightarrow 0$ while $v_{\perp}^{(+)} \rightarrow \sqrt{g'_1 \bar{n}/m}$. For the solid curves (where $\tilde{U}_1 = 1/4$), the speed of sound in the negative branch $v_{\perp}^{(-)}$ becomes

zero at $\tilde{U}_2 \simeq 37$, consistent with the value at which the dressed magnetization s'_z becomes unity for this choice of parameters. This signifies an instability toward the formation of a different phase.

The condition that the speed of sound must be non-negative imposes the constraint $D_2 \geq 0$. This condition marks the onset of a phase transition at the critical point $\tilde{g}_{12}^{(c)} = \sqrt{\tilde{g}'_1 \tilde{g}'_2}$, which does not depend on any cavity-mediated interaction parameters and is solely determined by the two-body interactions and $\tilde{\Omega}_R$. This critical point is not consistent with the previous results obtained from the variational approach, the effective low-energy GP equations in the SP, or the elementary excitations in the PW which all consistently predict a critical point for the PWP-SP phase transition that depends on the cavity-mediated interaction parameters. To verify that there was not an error in the calculations, the elementary excitations were computed directly in momentum space by Fourier transferring the effective low-energy Hamiltonian (30), and treating the fluctuations around the condensate $\varphi_{\tau'}(\mathbf{q} = 0)$ to second order in $\hat{\varphi}_{\tau'}(\mathbf{q})$ for small momenta \mathbf{q} . The results were identical with the real-space analysis, Eq. (42). Interestingly, the critical inter-species interaction $\tilde{g}_{12}^{(c)}$ above defines a phase boundary between the stripe phase and a phase-separated state in Raman-induced spin-orbit coupled BECs [14]. It is therefore conceivable that there is another phase between the SP and the PWP induced by the cavity interactions, whose signature is the observed inconsistency in the critical point.

IV. DISCUSSION AND CONCLUSIONS

In this work we have shown that cavity-mediated long-range interactions between atoms can profoundly alter the nature of the ground state and the elementary excitations of a cavity-induced spin-orbit-coupled two-component BEC, for ring-type cavities in the weak-coupling regime. Specifically, experimentally tunable cavity-mediated interactions compete with the standard two-body interactions to yield both plane-wave and stripe phase ground states. Indeed, positive long-range cavity interactions can stabilize fully attractive BECs (condensates where intra-species collisional interactions are negative, independent of the sign of the inter-species interaction) against collapse in the stripe phase. The collective excitations of the plane-wave phase ground states are found to have a distinctive roton-type excitation spectrum reminiscent of that of superfluid ^4He , which can be used as a signature of the phase. The stripe phase has a standard linear dispersion relation; the associated speed of sound is found to go negative at a critical value of the cavity interaction strength, signalling an instability toward another (likely phase-separated) phase. The results suggest that cavity QED, even in the weak-coupling regime, can yield interesting new physics for spin-orbit coupled BECs.

The results raise interesting avenues for future investigations. This work assumed a fictional experimental configuration where the momentum is a good quantum number in the direction of the applied spin-orbit interactions. In reality the condensate would be confined in this direction, and even a weak harmonic potential could change the physics. While the stripe phase would likely remain robust, as it is essentially a weak standing wave superimposed on the background condensate density profile, the plane-wave phase has no analog in a confined geometry. Another loose end is the nature of the phase hinted at in the limit of a large difference $\delta\tilde{U}$ between the cavity-mediated interactions between the two kinds of spin components \tilde{U}_1 and \tilde{U}_2 . For large $\delta\tilde{U}$, the sound velocity in the stripe phase was found to go negative, a signature of the dynamic instability of the phase. While other work suggests that this signals a

However, a few intriguing issues and questions remain unclear and deserve further investigations. These include the inconsistency in the critical phase transition point, how the combined SO coupling effect, the two-body interactions, and the cavity-mediated long-ranged

interactions change the superfluid–Mott-insulator phase transition as well as the nature of magnetic orders in the Mott-insulating regime when an optical lattice imposed inside the cavity. Furthermore, whether it is possible to have a superfluid–Mott-insulator-like phase transition with solely the cavity-mediated long-range interactions, whether there is more interesting physics in strong-coupling regime, and how the cavity fields are affected by the atoms. Some of these questions are the subject of our current works with some promising preliminary results and will be published elsewhere.

Acknowledgments

The authors are grateful to Paul Barclay and Christoph Simon for constructive criticisms. We also thank Han Pu and Lin Dong for stimulating correspondence. This work was supported by the Natural Sciences and Engineering Research Council of Canada and Alberta Innovates-Technology Futures.

Appendix A: Adiabatic Elimination of the Atomic Excited State

We first express the single-particle Hamiltonian density $\mathcal{H}^{(1)}$, Eq. (1), in the rotating frame of pump lasers [29] by applying the unitary transformation

$$\mathcal{U}_1 = \exp \left\{ i \left[\left(\hat{A}_1^\dagger \hat{A}_1 - \sigma_{aa} \right) \omega_{p1} + \left(\hat{A}_2^\dagger \hat{A}_2 - \sigma_{bb} \right) \omega_{p2} \right] t \right\},$$

to obtain

$$\begin{aligned} \mathcal{H}^{(1)} = & \left[\frac{\mathbf{p}^2}{2m} + V_{\text{ext}}(\mathbf{r}) \right] I_{3 \times 3} + \frac{\hbar \delta'}{2} (\sigma_{aa} - \sigma_{bb}) - \frac{\hbar}{2} (\Delta_{a1} + \Delta_{a2}) \sigma_{ee} + \hbar \left[\left(\mathcal{G}_{ae} e^{ik_R z} \hat{A}_1 \sigma_{ea} + \mathcal{G}_{be} e^{-ik_R z} \hat{A}_2 \sigma_{eb} \right) + \text{H.c.} \right] \\ & - \hbar (\Delta_{c1} \hat{A}_1^\dagger \hat{A}_1 + \Delta_{c2} \hat{A}_2^\dagger \hat{A}_2) + i\hbar \left[(\eta_1 \hat{A}_1^\dagger + \eta_2 \hat{A}_2^\dagger) - \text{H.c.} \right], \end{aligned} \quad (\text{A1})$$

where we have defined the atomic and the two-photon (or relative-atomic) detunings

$$\Delta_{a1} = \omega_{p1} - \frac{1}{\hbar} (\varepsilon_e - \varepsilon_a), \quad \Delta_{a2} = \omega_{p2} - \frac{1}{\hbar} (\varepsilon_e - \varepsilon_b), \quad \delta' = (\omega_{p1} - \omega_{p2}) - \frac{1}{\hbar} (\varepsilon_b - \varepsilon_a) = \Delta_{a1} - \Delta_{a2}, \quad (\text{A2a})$$

and cavity detunings

$$\Delta_{cj} = \omega_{pj} - \omega_j, \quad j = 1, 2, \quad (\text{A2b})$$

with respect to the pump lasers. Let us now assume that the detunings $\Delta_1 = \omega_1 - \varepsilon_{ea}/\hbar = -\Delta_{c1} + \Delta_{a1}$ and $\Delta_2 = \omega_2 - \varepsilon_{eb}/\hbar = -\Delta_{c2} + \Delta_{a2}$ are large compared to $\varepsilon_{ba}/\hbar = (\varepsilon_b - \varepsilon_a)/\hbar$ so that we can adiabatically eliminate the dynamic of the atomic excited state $|e\rangle$ from the Hamiltonian (A1) and obtain an effective Hamiltonian for the ground pseudospins $\{1, 2\} \equiv \{b, a\}$. Following the standard adiabatic elimination procedure [23, 35], we first find the Heisenberg equations of motion $i\hbar \dot{\sigma}_{e\tau} = [\sigma_{e\tau}, \mathcal{H}^{(1)}]$ for $\dot{\sigma}_{ea}$ and $\dot{\sigma}_{eb}$, and then (after transferring to slowly rotating variables) set them equal to zero to find the steady-state solutions $\sigma_{ea}^{(ss)}$ and $\sigma_{eb}^{(ss)}$. After substituting these steady-state solutions back in $\mathcal{H}^{(1)}$ (A1) and dropping terms diagonal in σ_{ee} , we arrive at the single-particle Hamiltonian density for pseudospins

$$\mathcal{H}_{\text{SO}}^{(1)} = \left[\frac{\mathbf{p}^2}{2m} + V_{\text{ext}}(\mathbf{r}) \right] \mathbb{I} + \hat{\varepsilon}_1 \sigma_{11} + \hat{\varepsilon}_2 \sigma_{22} + \hbar \Omega'_R \left(e^{2ik_R z} \hat{A}_2^\dagger \hat{A}_1 \sigma_{12} + e^{-2ik_R z} \hat{A}_1^\dagger \hat{A}_2 \sigma_{21} \right) + H'_{\text{cav}}, \quad (\text{A3})$$

where

$$H'_{\text{cav}} = -\hbar(\Delta_{c1}\hat{A}_1^\dagger\hat{A}_1 + \Delta_{c2}\hat{A}_2^\dagger\hat{A}_2) + i\hbar\left[\left(\eta_1\hat{A}_1^\dagger + \eta_2\hat{A}_2^\dagger\right) - \text{H.c.}\right],$$

and

$$\hat{\varepsilon}_1 = -\frac{\hbar\delta'}{2} + \frac{2\hbar\mathcal{G}_{be}^2}{\Delta_2}(\hat{A}_2^\dagger\hat{A}_2 + \frac{1}{2}), \quad \hat{\varepsilon}_2 = \frac{\hbar\delta'}{2} + \frac{2\hbar\mathcal{G}_{ae}^2}{\Delta_1}(\hat{A}_1^\dagger\hat{A}_1 + \frac{1}{2}). \quad (\text{A4})$$

Here, $\Omega'_R = \frac{\Delta_1 + \Delta_2}{\Delta_1\Delta_2}\mathcal{G}_{ae}\mathcal{G}_{be}$ is the two-photon Rabi frequency and $\mathbb{I} \equiv I_{2 \times 2}$ is the identity matrix in the pseudospin space. Note the hat on $\hat{\varepsilon}_\tau$, implying that it depends on the cavity field operators. After transferring to the co-moving frame of the cavity modes by applying the unitary transformation $\mathcal{U}_2 = e^{-ik_R(\sigma_{11} - \sigma_{22})z}$ to the Hamiltonian density (A3), we obtain the SO-coupled single-particle Hamiltonian density

$$\mathcal{H}_{\text{SO}}''^{(1)} = \frac{1}{2m} \left\{ p_\perp^2 \mathbb{I} + [p_z \mathbb{I} - \hbar k_R(\sigma_{22} - \sigma_{11})]^2 \right\} + V_{\text{ext}}(\mathbf{r})\mathbb{I} + \sum_{\tau=1,2} \hat{\varepsilon}_\tau \sigma_{\tau\tau} + \hbar\Omega'_R \left(\hat{A}_2^\dagger \hat{A}_1 \sigma_{12} + \hat{A}_1^\dagger \hat{A}_2 \sigma_{21} \right) + H'_{\text{cav}}. \quad (\text{A5})$$

One can identify $\hbar k_R(\sigma_{22} - \sigma_{11})$ with eA_z^*/c as in the minimal coupling Hamiltonian, that is, $eA_z^*/c \equiv \hbar k_R(\sigma_{22} - \sigma_{11}) = -\hbar k_R \sigma_z$, where $\sigma_z = \sigma_{11} - \sigma_{22}$ is the third Pauli matrix. Nonetheless, we emphasize that here A_z^* is a matrix acting in the internal pseudospin states, in contrast to the ordinary vector potential whose components are scalar fields. Then the single-particle Hamiltonian reads

$$H_{\text{SO}}''^{(1)} = \frac{1}{2m} \int \hat{\Psi}^\dagger \left[p_\perp^2 \mathbb{I} + (p_z \mathbb{I} + \hbar k_R \sigma_z)^2 + V_{\text{ext}}(\mathbf{r})\mathbb{I} \right] \hat{\Psi} d^3r + \sum_{\tau=1,2} \hat{\varepsilon}_\tau \hat{N}_\tau + \hbar\Omega'_R \left(\hat{A}_2^\dagger \hat{A}_1 \hat{S}_+ + \hat{A}_1^\dagger \hat{A}_2 \hat{S}_- \right) + H'_{\text{cav}}, \quad (\text{A6})$$

where $\hat{\Psi}(\mathbf{r}) = (\hat{\psi}_1(\mathbf{r}), \hat{\psi}_2(\mathbf{r}))^\top$ are the bosonic field operators, $\hat{N}_\tau = \int \hat{\psi}_\tau^\dagger(\mathbf{r})\hat{\psi}_\tau(\mathbf{r})d^3r$ is the total atomic number operator for pseudospin τ , $\hat{N} = \hat{N}_1 + \hat{N}_2$ is the total atomic number operator, and $\hat{S}_+ = \hat{S}_-^\dagger = \int \hat{\psi}_1^\dagger(\mathbf{r})\hat{\psi}_2(\mathbf{r})d^3r$ are the collective pseudospin raising and lowering operators.

Appendix B: Adiabatic Elimination of the Cavity Fields

By noting that the cavity field operator commutes with the atomic interaction Hamiltonian $[\hat{A}, H_{\text{int}}] = 0$, then the Heisenberg equations of motion of the cavity field operators are determined by the single-particle Hamiltonian $H_{\text{SO}}''^{(1)}$, Eq. (A6): $\partial_t \hat{A}_j = -i[\hat{A}_j, H_{\text{SO}}''^{(1)}]/\hbar - \kappa \hat{A}_j$, where the cavity-mode decay $-\kappa \hat{A}_j$ is included phenomenologically. They can be recast in the matrix form,

$$\frac{d}{dt} \begin{pmatrix} \hat{A}_1 \\ \hat{A}_2 \end{pmatrix} = i \begin{pmatrix} \hat{\alpha}_{11} & -\hat{\alpha}_{12} \\ -\hat{\alpha}_{21} & \hat{\alpha}_{22} \end{pmatrix} \begin{pmatrix} \hat{A}_1 \\ \hat{A}_2 \end{pmatrix} + \begin{pmatrix} \eta_1 \\ \eta_2 \end{pmatrix}, \quad (\text{B1})$$

where the elements of the "operator" matrix $\hat{\alpha}$ are given by

$$\hat{\alpha}_{11} = (\Delta_{c1} + i\kappa) - \frac{2\mathcal{G}_{ae}^2}{\Delta_1} \hat{N}_2, \quad \hat{\alpha}_{22} = (\Delta_{c2} + i\kappa) - \frac{2\mathcal{G}_{be}^2}{\Delta_2} \hat{N}_1, \quad \hat{\alpha}_{12} = \hat{\alpha}_{21}^\dagger = \Omega'_R \hat{S}_-. \quad (\text{B2})$$

If the cavity decay rate κ is large, then the cavity fields reach steady states very quickly. By setting $\partial_t \hat{A}_1 = \partial_t \hat{A}_2 = 0$ in Eq. (B1), one can simultaneously solve the two equations of motion to obtain formal expressions for the steady-state field amplitudes $\hat{A}_{\text{ss}j}$. However, one should take special care in solving these equations since the cavity fields and atomic fields commute with one another and this can give rise to ambiguities in solving these equations. In order to avoid such ambiguities, we symmetrize the equations of motion and exercise symmetrization procedure in all results following from the equations of motion. Thus, after setting $\partial_t \hat{A}_1 = \partial_t \hat{A}_2 = 0$ in Eq. (B1), we re-express equations of motion as

$$\frac{i}{2} \left(\hat{\alpha}_{11} \hat{A}_{\text{ss}1} + \hat{A}_{\text{ss}1} \hat{\alpha}_{11} \right) - \frac{i}{2} \left(\hat{\alpha}_{12} \hat{A}_{\text{ss}2} + \hat{A}_{\text{ss}2} \hat{\alpha}_{12} \right) + \eta_1 = \frac{i}{2} \left(\hat{\alpha}_{22} \hat{A}_{\text{ss}2} + \hat{A}_{\text{ss}2} \hat{\alpha}_{22} \right) - \frac{i}{2} \left(\hat{\alpha}_{21} \hat{A}_{\text{ss}1} + \hat{A}_{\text{ss}1} \hat{\alpha}_{21} \right) + \eta_2 = 0. \quad (\text{B3})$$

Equation (B3) can then be rearranged

$$\hat{A}_{\text{ss1}} = \frac{1}{4} \left[(\hat{\alpha}_{11}^{-1} \hat{\alpha}_{12} + \hat{\alpha}_{12} \hat{\alpha}_{11}^{-1}) \hat{A}_{\text{ss2}} + \hat{A}_{\text{ss2}} (\hat{\alpha}_{11}^{-1} \hat{\alpha}_{12} + \hat{\alpha}_{12} \hat{\alpha}_{11}^{-1}) \right] + i \hat{\alpha}_{11}^{-1} \eta_1, \quad (\text{B4a})$$

$$\hat{A}_{\text{ss2}} = \frac{1}{4} \left[(\hat{\alpha}_{22}^{-1} \hat{\alpha}_{21} + \hat{\alpha}_{21} \hat{\alpha}_{22}^{-1}) \hat{A}_{\text{ss1}} + \hat{A}_{\text{ss1}} (\hat{\alpha}_{22}^{-1} \hat{\alpha}_{21} + \hat{\alpha}_{21} \hat{\alpha}_{22}^{-1}) \right] + i \hat{\alpha}_{22}^{-1} \eta_2, \quad (\text{B4b})$$

where $\hat{\alpha}_{11}^{-1}$ and $\hat{\alpha}_{22}^{-1}$ are the inverse operators of $\hat{\alpha}_{11}$ and $\hat{\alpha}_{22}$, respectively, such that $\hat{\alpha}_{11} \hat{\alpha}_{11}^{-1} = \hat{\alpha}_{11}^{-1} \hat{\alpha}_{11} = \hat{1}$ and $\hat{\alpha}_{22} \hat{\alpha}_{22}^{-1} = \hat{\alpha}_{22}^{-1} \hat{\alpha}_{22} = \hat{1}$. In order to make the subsequent analyses somewhat easier and trackable, we assume that all dual variables (except η_j at this moment) are equal, namely, $\Delta_1 = \Delta_2 \equiv \Delta$, $\Delta_{c1} = \Delta_{c2} \equiv \Delta_c$, and $\mathcal{G}_{ae} = \mathcal{G}_{be} \equiv \mathcal{G}_0$. We also introduce $\tilde{\Delta}_c \equiv \Delta_c + i\kappa$ for a shorthand. We expand the inverse operators to the second order in a small unitless parameter $\xi \equiv 2\mathcal{G}_0^2/\Delta\tilde{\Delta}_c \ll 1$ (and with $\langle \hat{N}_\tau \rangle \sim 10^5$ one still has $\xi \langle \hat{N}_\tau \rangle \sim 10^{-2} \ll 1$, see Sec. II for more details),

$$\begin{aligned} \hat{\alpha}_{11}^{-1} &= \left(\tilde{\Delta}_c - \frac{2\mathcal{G}_0^2}{\Delta} \hat{N}_2 \right)^{-1} \simeq \tilde{\Delta}_c^{-1} \left(1 + \frac{2\mathcal{G}_0^2}{\Delta\tilde{\Delta}_c} \hat{N}_2 + \frac{4\mathcal{G}_0^4}{\Delta^2\tilde{\Delta}_c^2} \hat{N}_2^2 \right), \\ \hat{\alpha}_{22}^{-1} &= \left(\tilde{\Delta}_c - \frac{2\mathcal{G}_0^2}{\Delta} \hat{N}_1 \right)^{-1} \simeq \tilde{\Delta}_c^{-1} \left(1 + \frac{2\mathcal{G}_0^2}{\Delta\tilde{\Delta}_c} \hat{N}_1 + \frac{4\mathcal{G}_0^4}{\Delta^2\tilde{\Delta}_c^2} \hat{N}_1^2 \right), \end{aligned} \quad (\text{B5})$$

such that $\hat{\alpha}_{11} \hat{\alpha}_{11}^{-1} = \hat{\alpha}_{11}^{-1} \hat{\alpha}_{11} = \hat{\alpha}_{22} \hat{\alpha}_{22}^{-1} = \hat{\alpha}_{22}^{-1} \hat{\alpha}_{22} = \hat{1} + \mathcal{O}(\xi^3)$. Note that the error in symmetrizing Eq. (B4) is also of order $\mathcal{O}(\xi^3)$. This can be easily checked by substituting, say, Eq. (B4a) in the first equation of (B3). Equations (B4a) and (B4b) can now be simultaneously solved, yielding

$$\begin{aligned} \hat{A}_{\text{ss1}} &= i\hat{\Gamma}^{-1} \left[\eta_1 \hat{\alpha}_{11}^{-1} + \frac{\eta_2}{4} (\hat{\alpha}_{11}^{-1} \hat{\alpha}_{12} \hat{\alpha}_{22}^{-1} + \hat{\alpha}_{12} \hat{\alpha}_{11}^{-1} \hat{\alpha}_{22}^{-1} + \hat{\alpha}_{22}^{-1} \hat{\alpha}_{11}^{-1} \hat{\alpha}_{12} + \hat{\alpha}_{22}^{-1} \hat{\alpha}_{12} \hat{\alpha}_{11}^{-1}) \right], \\ \hat{A}_{\text{ss2}} &= i\hat{\Gamma}^{-1} \left[\eta_2 \hat{\alpha}_{22}^{-1} + \frac{\eta_1}{4} (\hat{\alpha}_{22}^{-1} \hat{\alpha}_{21} \hat{\alpha}_{11}^{-1} + \hat{\alpha}_{21} \hat{\alpha}_{22}^{-1} \hat{\alpha}_{11}^{-1} + \hat{\alpha}_{11}^{-1} \hat{\alpha}_{22}^{-1} \hat{\alpha}_{21} + \hat{\alpha}_{11}^{-1} \hat{\alpha}_{21} \hat{\alpha}_{22}^{-1}) \right], \end{aligned} \quad (\text{B6})$$

where $\hat{\Gamma} = \left[1 - \frac{1}{2\tilde{\Delta}_c^2} (\hat{\alpha}_{12} \hat{\alpha}_{21} + \hat{\alpha}_{21} \hat{\alpha}_{12}) \right]$ up to ξ^2 , by noting $\hat{\alpha}_{12} = \hat{\alpha}_{21}^\dagger \propto \Omega'_R = 2\mathcal{G}_0^2/\Delta$ and (B5). We then have

$$\hat{\Gamma}^{-1} \simeq 1 + \frac{1}{2\tilde{\Delta}_c^2} (\hat{\alpha}_{12} \hat{\alpha}_{21} + \hat{\alpha}_{21} \hat{\alpha}_{12}) = 1 + \frac{2\mathcal{G}_0^4}{\Delta^2\tilde{\Delta}_c^2} (\hat{S}_+ \hat{S}_- + \hat{S}_- \hat{S}_+), \quad (\text{B7})$$

up to $\mathcal{O}(\xi^3)$. Using Eqs. (B2), (B5)-(B7), and retaining terms up to ξ^2 , we obtain

$$\begin{aligned} \hat{A}_{\text{ss1}} &= \frac{i}{\tilde{\Delta}_c} \left\{ \eta_1 + \frac{2\mathcal{G}_0^2}{\Delta\tilde{\Delta}_c} (\eta_1 \hat{N}_2 + \eta_2 \hat{S}_-) + \frac{4\mathcal{G}_0^4}{\Delta^2\tilde{\Delta}_c^2} \left[\eta_1 \hat{N}_2^2 + \frac{\eta_1}{2} (\hat{S}_+ \hat{S}_- + \hat{S}_- \hat{S}_+) + \eta_2 \hat{N} \hat{S}_- \right] \right\}, \\ \hat{A}_{\text{ss2}} &= \frac{i}{\tilde{\Delta}_c} \left\{ \eta_2 + \frac{2\mathcal{G}_0^2}{\Delta\tilde{\Delta}_c} (\eta_2 \hat{N}_1 + \eta_1 \hat{S}_+) + \frac{4\mathcal{G}_0^4}{\Delta^2\tilde{\Delta}_c^2} \left[\eta_2 \hat{N}_1^2 + \frac{\eta_2}{2} (\hat{S}_+ \hat{S}_- + \hat{S}_- \hat{S}_+) + \eta_1 \hat{N} \hat{S}_+ \right] \right\}. \end{aligned} \quad (\text{B8})$$

By substituting steady-state solutions (B8) and their Hermitian conjugates in the Hamiltonian $H_{\text{SO}}''^{(1)}$, Eq. (A6), exercising symmetrization procedure again and retaining terms up to ξ^2 , we can find an effective Hamiltonian which depends solely on the atomic operators. After some tedious though straightforward algebra, we obtain the cavity-field-eliminated effective many-body Hamiltonian

$$H_{\text{eff}} = \int d^3r \left(\hat{\Psi}^\dagger \mathcal{H}_{\text{SO}}^{(1)} \hat{\Psi} + \frac{1}{2} g_1 \hat{n}_1^2 + \frac{1}{2} g_2 \hat{n}_2^2 + g_{12} \hat{n}_1 \hat{n}_2 \right) + \sum_{\tau=1,2} U_\tau \hat{N}_\tau^2 + (U_\pm \hat{S}_+ \hat{S}_- + U_\mp \hat{S}_- \hat{S}_+) + 2U_{\text{ds}} \hat{N} \hat{S}_x, \quad (\text{B9})$$

where the cavity-field-eliminated, effective single-particle Hamiltonian density takes the familiar form

$$\mathcal{H}_{\text{SO}}^{(1)} = -\frac{\hbar^2}{2m} [\nabla_\perp^2 - (-i\partial_z + k_R \sigma_z)^2] + V_{\text{ext}}(\mathbf{r}) + \frac{1}{2} \hbar \delta \sigma_z + \hbar \Omega_R \sigma_x, \quad (\text{B10})$$

with effective two-photon detuning and Raman coupling given by

$$\begin{aligned} \delta &\equiv \frac{2\mathcal{G}_0^2(\Delta_c^2 - \kappa^2)}{\Delta(\Delta_c^2 + \kappa^2)^2} (\eta_2^2 - \eta_1^2), \\ \Omega_R &= \frac{2\mathcal{G}_0^2}{\Delta(\Delta_c^2 + \kappa^2)^2} \left(\Delta_c^2 - \kappa^2 - \frac{2\mathcal{G}_0^2 \Delta_c}{\Delta} \right) \eta_1 \eta_2 = \frac{\Omega'_R}{(\Delta_c^2 + \kappa^2)^2} \left(\Delta_c^2 - \kappa^2 - \frac{2\mathcal{G}_0^2 \Delta_c}{\Delta} \right) \eta_1 \eta_2. \end{aligned} \quad (\text{B11})$$

(Note that $\delta' = 0$, since we have assumed $\Delta_{a1} = \Delta_{a2} \equiv \Delta_a$; cf. Eqs. (A2) and (A4).) The coefficients of the cavity-mediated long-range interactions are found to be

$$U_1 = \frac{4\hbar\mathcal{G}_0^4\Delta_c(\Delta_c^2 - 3\kappa^2)}{\Delta^2(\Delta_c^2 + \kappa^2)^3}\eta_2^2, \quad U_2 = \frac{4\hbar\mathcal{G}_0^4\Delta_c(\Delta_c^2 - 3\kappa^2)}{\Delta^2(\Delta_c^2 + \kappa^2)^3}\eta_1^2, \quad U_{ds} = \frac{4\hbar\mathcal{G}_0^4\Delta_c(\Delta_c^2 - 3\kappa^2)}{\Delta^2(\Delta_c^2 + \kappa^2)^3}\eta_1\eta_2, \\ U_{\pm} = \frac{4\hbar\mathcal{G}_0^4\Delta_c}{\Delta^2(\Delta_c^2 + \kappa^2)^3} [\Delta_c^2\eta_1^2 - (\eta_1^2 + 2\eta_2^2)\kappa^2], \quad U_{\mp} = \frac{4\hbar\mathcal{G}_0^4\Delta_c}{\Delta^2(\Delta_c^2 + \kappa^2)^3} [\Delta_c^2\eta_2^2 - (\eta_2^2 + 2\eta_1^2)\kappa^2]. \quad (\text{B12})$$

The terms with coefficients $U_{1/2}$, $U_{\pm/\mp}$, and U_{ds} in the effective Hamiltonian (B9) are the cavity-mediated long-range interactions. Note that in the special case of $\eta_1 = \eta_2 \equiv \eta$, one has $\delta = 0$ and $U_1 = U_2 = U_{\pm} = U_{\mp} = U_{ds} \equiv U$.

-
- [1] M. H. Anderson, J. R. Ensher, M. R. Matthews, C. E. Wieman, and E. A. Cornell, *Science* **269**, 198 (1995).
[2] K. Davis, M.-O. Mewes, M. R. Andrews, N. J. van Druten, D. S. Durfee, D. M. Kurn, and W. Ketterle, *Phys. Rev. Lett.* **75**, 3969 (1995).
[3] I. Bloch, J. Dalibard, and W. Zwerger, *Rev. Mod. Phys.* **80**, 885 (2008).
[4] M. Lewenstein, A. Sanpera, V. Ahufinger, B. Damski, A. Sen(De), and U. Sen, *Advances in Physics* **56**, 243 (2007).
[5] M. Greiner, O. Mandel, T. Esslinger, T. W. Hänsch, and I. Bloch, *Nature* **415**, 39 (2002).
[6] J. Dalibard, F. Gerbier, G. Juzeliūnas, and P. Öhberg, *Rev. Mod. Phys.* **83**, 1523 (2011).
[7] Y.-J. Lin, R. L. Compton, K. Jiménez-García, J. V. Porto, and I. B. Spielman, *Nature* **462**, 628 (2009).
[8] Y.-J. Lin, K. Jiménez-García, and I. B. Spielman, *Nature* **471**, 83 (2011).
[9] X.-L. Qi and S.-C. Zhang, *Rev. Mod. Phys.* **83**, 1057 (2011).
[10] C. Wang, C. Gao, C.-M. Jian, and H. Zhai, *Phys. Rev. Lett.* **105**, 160403 (2010).
[11] T.-L. Ho and S. Zhang, *Phys. Rev. Lett.* **107**, 150403 (2011).
[12] Y. Li, L. P. Pitaevskii, and S. Stringari, *Phys. Rev. Lett.* **108**, 225301 (2012).
[13] W. Zheng and Z. Li, *Phys. Rev. A* **85**, 053607 (2012).
[14] Q.-Q. Lü and D. E. Sheehy, *Phys. Rev. A* **88**, 043645 (2013).
[15] R. Liao, O. Fialko, J. Brand, and U. Zülicke, preprint arXiv:1504.07370 (2015).
[16] W. S. Cole, S. Zhang, A. Paramekanti, and N. Trivedi, *Phys. Rev. Lett.* **109**, 085302 (2012).
[17] J. Radić, A. D. Cioło, K. Sun, and V. Galitski, *Phys. Rev. Lett.* **109**, 085303 (2012).
[18] Z. Cai, X. Zhou, and C. Wu, *Phys. Rev. A* **85**, 061605(R) (2012).
[19] T. Graß, K. Saha, K. Sengupta, and M. Lewenstein, *Phys. Rev. A* **84**, 053632 (2011).
[20] H. J. Kimble, *Physica Scripta* **T76**, 127 (1998).
[21] H. Ritsch, P. Domokos, F. Brennecke, and T. Esslinger, *Rev. Mod. Phys.* **85**, 553 (2013).
[22] K. Baumann, C. Guerlin, F. Brennecke, and T. Esslinger, *Nature* **464**, 1301 (2010).
[23] F. Mivehvar and D. L. Feder, *Phys. Rev. A* **89**, 013803 (2014).
[24] L. Dong, L. Zhou, B. Wu, B. Ramachandhran, and H. Pu, *Phys. Rev. A* **89**, 011602(R) (2014).
[25] Y. Deng, J. Cheng, H. Jing, , and S. Yi, *Phys. Rev. Lett.* **112**, 143007 (2014).
[26] L. Dong, C. Zhu, and H. Pu, e-print: arXiv:1504.01729 (2015).
[27] B. Padhi and S. Ghosh, *Phys. Rev. A* **90**, 023627 (2014).
[28] The applied frequencies are assumed to be $\omega_1 = \omega_2 + \Delta\omega$ with $|\Delta\omega|/\omega_j \ll 1$. In the general case when $k_1 \neq k_2$, one can define $k_c \equiv \frac{1}{2}(k_1 + k_2)$ and $\Delta k_c \equiv k_1 - k_2$. All the results still hold, except that p_z is replaced by $p_z - \frac{1}{2}\hbar\Delta k_c$ after transferring to the co-moving frame of the cavity modes, which is just a Galilean transformation of the momentum.
[29] C. Maschler, I. Mekhov, and H. Ritsch, *Eur. Phys. J. D* **46**, 545 (2008).
[30] A. L. Gaunt, T. F. Schmidutz, I. Gotlibovych, R. P. Smith, and Z. Hadzibabic, *Phys. Rev. Lett.* **110**, 200406 (2013).
[31] P. Meystre and M. Sargent, *Elements of Quantum Optics, 3rd. ed.* (Springer, Berlin, 1999).
[32] P. Münstermann, T. Fischer, P. Maunz, P. W. H. Pinkse, and G. Rempe, *Phys. Rev. Lett.* **84**, 4068 (2000).
[33] F. Brennecke, T. Donner, S. Ritter, T. Bourdel, M. Köhl, and T. Esslinger, *Nature* **450**, 268 (2007).
[34] T. D. Stanescu, B. Anderson, and V. Galitski, *Phys. Rev. A* **78**, 023616 (2008).
[35] C. C. Gerry and J. H. Eberly, *Phys. Rev. A* **42**, 6805 (1990).